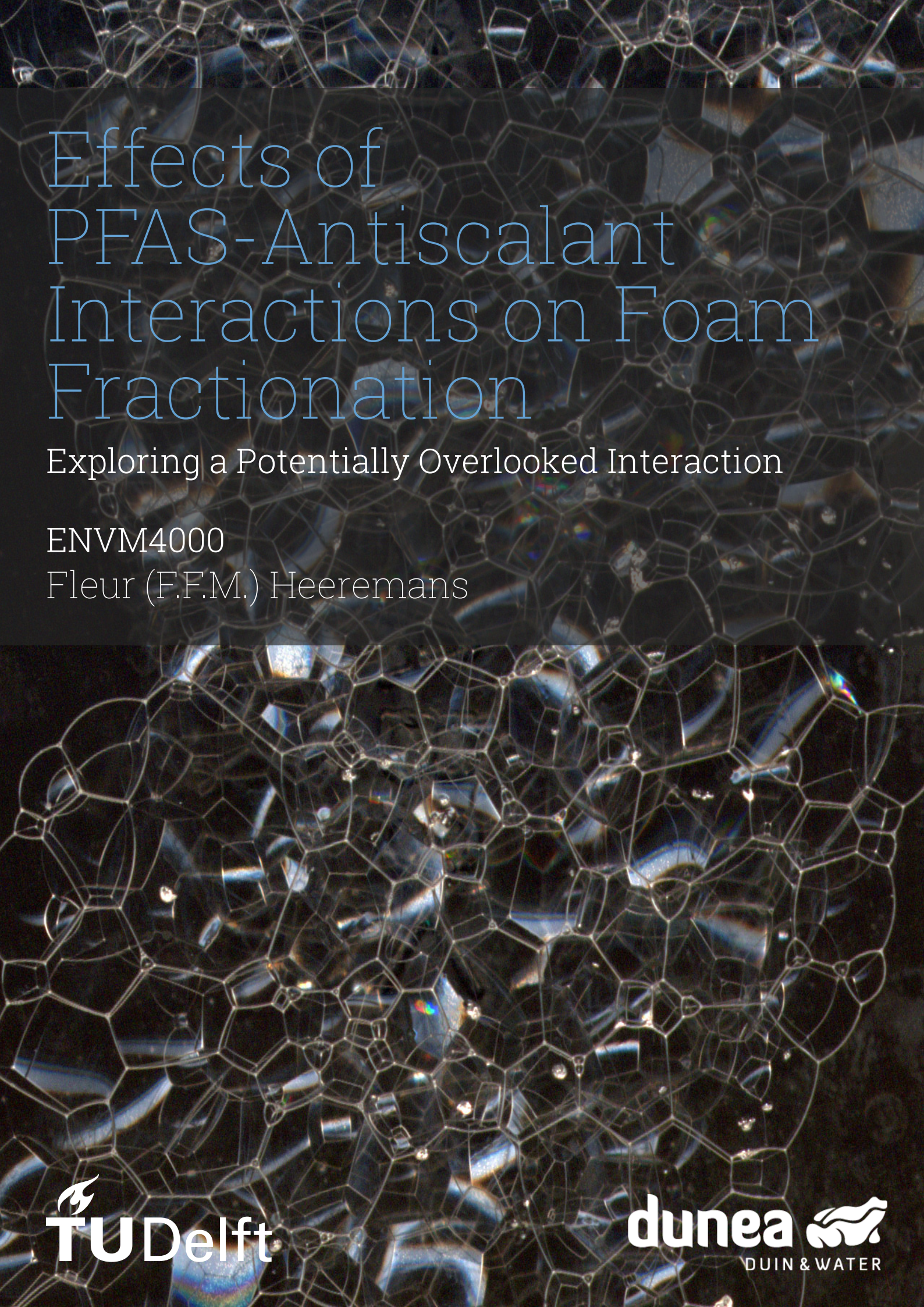

Effects of PFAS-Antiscalant Interactions on Foam Fractionation

Exploring a Potentially Overlooked Interaction

ENVM4000

Fleur (F.F.M.) Heeremans

TU Delft

dunea DUIN & WATER

Effects of PFAS-Antiscalant Interactions on Foam Fractionation

Exploring a Potentially Overlooked Interaction

by

Fleur (F.F.M.) Heeremans

to obtain the degree of Master of Science

at the Delft University of Technology.

Student number:	4718186
Project duration:	February 2 - July 16, 2026
Thesis committee:	Dr. ir. S. J. Smith
	Prof. dr. ir. D. van Halem
	Dr. B. M. van Breukelen
	Ir. S. van der Poel
	Ir. G. Florentinus

Cover: André Karwath (Modified)

TU Delft

Preface

First and foremost, I would like to express my sincere gratitude to my entire thesis committee. It has been a highly educational and inspiring experience to be guided by a group of people with such extensive knowledge in a field that interests me so deeply. I knew early on that I wanted to focus my thesis research on PFAS, and it did not take long to bring together the right people for this project. In my view, PFAS represents one of the greatest risks currently facing humanity. For that reason, I am grateful that, through this research, I may have been able to make a small contribution toward a future solution.

I would like to extend a special word of thanks to Dr. ir. S. J. Smith, the chair of my thesis committee and my day-to-day advisor. You provided me with the guidance, structure, and tools I needed throughout this research. I greatly appreciated our weekly meetings; even when I felt overwhelmed beforehand, I always left them feeling positive and motivated to continue.

I would also like to thank Ir. S. van der Poel and Ir. G. Florentinus for the excellent guidance and support you provided during my time at Dunea. It was a pleasure to work with you and with Dunea, not only because the collaboration ran smoothly and the research was feasible, but also because of the support I received along the way, initially mainly from Ir. S. van der Poel, and later from Ir. G. Florentinus as well. I am also grateful to Dr. B. M. van Breukelen for his valuable advice and for offering a broader perspective on the subject. His perspective from a slightly different sector often provided new insights, which was very helpful throughout the process. Furthermore, I would like to thank Prof. dr. ir. D. van Halem for her collaboration and for making this team and project possible. The brainstorming sessions at the start of my project, as well as your help in bringing this team together, were very valuable. Later in the process, your feedback and advice also helped me to move forward.

The past few months have been a major learning process, during which I felt I was truly able to express myself. I have often described this period to my friends as the best part of my studies. This was, of course, also thanks to the many enjoyable coffee breaks with my fellow graduating students. It was very valuable to go through this process alongside people who were going through a similar process, and to be able to talk things through now and then.

Finally, I would like to thank Papa, Mama, and Daan. The many phone calls and conversations were a great source of support. I am grateful that you were always willing to listen, even at times when you did not fully understand what I was talking about.

Fleur (F.F.M.) Heeremans
Delft, August 2026

Summary

PFAS are a growing concern for drinking water treatment because of their persistence, mobility and potential health risks. Reverse osmosis (RO) is an effective technology for PFAS removal, but it produces a concentrate stream in which PFAS and other dissolved compounds accumulate. This concentrate requires further treatment to prevent the PFAS problem from being transferred to another waste stream. Foam fractionation is a promising option for this type of stream because it uses the surface-active properties of PFAS. During foam fractionation, PFAS adsorb to the air-water interface of rising bubbles and are transported to the foam phase, producing a relatively small foamate stream with elevated PFAS concentrations.

Previous research reported high PFAS removal efficiencies during foam fractionation of membrane concentrate containing antiscalant. It was suggested that the antiscalant present in the concentrate may have contributed to this improved performance. Antiscalants are added to RO systems to prevent scaling and are largely retained in the concentrate stream. Because many antiscalants are polymeric or contain anionic functional groups, they may interact with PFAS, dissolved ions or the air-water interface. However, it remains unclear whether such interactions influence PFAS removal and enrichment during foam fractionation. Therefore, this study investigated the effect of different antiscalants on PFAS removal from RO concentrate.

All experiments were performed with RO concentrate from Dunea's UF/RO pilot. The concentrate was collected on one day and in one batch to minimise differences in water composition between experiments. Six commercial antiscalants were tested: 4Aqua OSM BD30, Ameroyal 363, Vitec 1141, Vitec 1200, Sokalan RO400 and Aquatreat 535. A control experiment without antiscalant was also performed. The antiscalants were dosed at 23.5 mg/L, based on the expected concentration in the RO concentrate when the RO system operates at 80% recovery. The foam fractionation experiments were carried out in a continuous column setup with a contact time of approximately 30 minutes and an airflow rate of 4 L/min. Samples were collected from the influent, effluent and foamate after steady-state operation had been reached. PFAS concentrations were measured using LC-MS. In addition, pH, conductivity, surface tension, viscosity and visual foam characteristics were evaluated.

The effect of antiscalants on foam formation and foam characteristics appeared limited. The surface tension of the control sample was 69.26 mN/m, while the antiscalant-containing samples showed slightly lower values between 66.73 and 67.96 mN/m. This indicates that antiscalants slightly lowered the surface tension of the RO concentrate. However, the differences between antiscalants were small. Viscosity values were almost identical for all samples, and visual observations did not show clear differences in foam height, bubble size or foam structure. Therefore, the tested antiscalants did not appear to strongly influence the visible foam characteristics under the applied conditions.

The mean ΣPFAS removal efficiencies ranged from 64.8% to 79.2%. The control experiment without antiscalant showed a removal efficiency of 71.8%. Most antiscalant-containing experiments showed slightly higher removal efficiencies than the control, except for V1141, which showed the lowest removal efficiency. However, the differences between experiments were relatively small. The results therefore do not show a clear or dominant improvement in total PFAS removal due to antiscalant addition under the applied conditions.

Mean ΣPFAS enrichment factors showed larger differences between experiments than removal efficiencies. The mean ΣPFAS enrichment factors ranged from 2.48 to 6.86, with the highest values observed for BD30 and V1141. This suggests that antiscalants may have influenced the partitioning of PFAS between the bulk liquid and the foam phase. However, the experiments with the highest enrichment factors also showed

larger deviations in mass balance closure. As a result, enrichment factors should be interpreted together with removal efficiencies and mass balance recoveries rather than as stand-alone performance indicators.

The compound-specific results showed that PFAS properties had a strong influence on foam fractionation performance. Long-chain PFAS were generally removed more efficiently than short-chain PFAS. This is expected because long-chain PFAS are more hydrophobic and more surface-active, causing them to adsorb more strongly to the air-water interface. Short-chain PFAS, such as PFBS, were more difficult to remove and showed lower enrichment. These results indicate that chain length and molecular structure are important factors in foam fractionation performance and may have a stronger influence than the specific antiscalant type.

The mechanism by which antiscalants may influence PFAS foam fractionation remains uncertain. Based on literature, possible mechanisms include changes in cation availability, electrostatic interactions, PFAS hydrophobicity, interfacial adsorption behaviour and foam film stability. Since most tested antiscalants are expected to be anionic, direct electrostatic attraction with anionic PFAS is not expected. Their effect is therefore more likely to be indirect and related to matrix effects. Such effects may be more relevant for short-chain PFAS, because their partitioning to the air-water interface is weaker and more sensitive to changes in water composition.

Several limitations should be considered when interpreting the results. Although one RO concentrate batch was used for all experiments, some matrix variability within this batch may still have occurred. In addition, PFAS analysis was performed in two batches. This may have contributed to analytical variability and is especially relevant for the interpretation of the V1141 experiment, for which the influent sample was analysed in a different batch from the effluent and foamate samples. The TOC data were also not sufficiently reliable to support a detailed interpretation of organic matter effects.

Overall, this study showed that foam fractionation can remove PFAS from RO concentrate, with removal efficiencies comparable to those reported in literature. The results suggest that antiscalants may have contributed to differences in PFAS enrichment and compound-specific behaviour, but no clear or dominant antiscalant effect could be confirmed. Antiscalants should therefore be considered as one possible matrix component that may influence foam fractionation performance, together with PFAS chain length, water composition, conductivity, foam stability and analytical uncertainty. Future research should include improved water quality characterisation, higher antiscalant concentrations and positive control experiments with a known cationic co-surfactant to better understand the mechanisms behind possible antiscalant effects.

Contents

Preface i

Summary ii

1 Introduction 1
- 1.1 Background and Context . . . 1
- 1.2 Problem Statement . . . 1
- 1.3 Positioning . . . 2
- 1.4 Research Question and Objectives . . . 3

2 Theoretical Background 4
- 2.1 Per- and Polyfluoroalkyl Substances (PFAS) . . . 4
  - 2.1.1 Classification . . . 4
  - 2.1.2 Surface Activity and Amphiphilic Structure of PFAS . . . 5
- 2.2 Reverse Osmosis as a PFAS Treatment Technology . . . 6
  - 2.2.1 Principle of Reverse Osmosis . . . 6
  - 2.2.2 Reverse Osmosis Membranes . . . 7
  - 2.2.3 PFAS Removal and Co-concentrates . . . 7
  - 2.2.4 Membrane Failure Mechanisms . . . 7
- 2.3 Membrane Antiscalants . . . 8
  - 2.3.1 Scale Inhibiting Mechanisms . . . 9
  - 2.3.2 Typical active ingredients of antiscalant . . . 9
- 2.4 Foam Fractionation . . . 10
  - 2.4.1 Foam Affecting Factors . . . 10
  - 2.4.2 Possible Influence on FF and PFAS Removal . . . 11

3 Methodology 13
- 3.1 Concentrate Stream . . . 13
- 3.2 Antiscalants . . . 13
  - 3.2.1 Antiscalant Dosing . . . 14
- 3.3 Experimental Setup and Approach . . . 15
  - 3.3.1 Experimental Setup Description . . . 15
  - 3.3.2 Experimental Parameters . . . 15
  - 3.3.3 Experimental Procedure . . . 16
- 3.4 Sampling . . . 16
  - 3.4.1 Sample analysis . . . 17
  - 3.4.2 Data Analysis and Processing . . . 18
  - 3.4.3 Additional Testing . . . 19

4 Results and Discussion 21
- 4.1 Influent Characteristics . . . 21
  - 4.1.1 Reverse Osmosis Concentrate . . . 21
  - 4.1.2 Field Blank . . . 22
- 4.2 Bulk Liquid Properties . . . 23
- 4.3 pH, Conductivity and TOC . . . 25

4.4 Overall Foam Fractionation Performance . . . 25
4.5 Compound-Specific Behaviour . . . 28
4.5.1 Compound-Specific Removal Efficiencies . . . 29
4.5.2 Compound-Specific Enrichment and Mass Balance Closure . . . 30
4.6 Potential Influence of Antiscalants on PFAS Foam Fractionation . . . 34

5 Conclusion and Recommendations **35**
5.1 Conclusion . . . 35
5.2 Recommendations . . . 36

References **37**

A Analytical Information and PFAS Classification **43**
A.1 PFAS Classification by Compound Group and Chain Length . . . 43
A.2 Limits of Quantification . . . 44
A.3 Calibration Curves and Calibration Ranges . . . 45

B Supplementary Compound Specific Results **46**
B.1 Additional Water Quality Results . . . 46
B.2 Compound-Specific PFAS Concentrations . . . 47
B.2.1 Individual PFAS Results . . . 47
B.2.2 Compound-Specific Removal Efficiencies . . . 49
B.2.3 Compound-Specific Enrichment Factors . . . 50
B.2.4 Compound-Specific Mass Balance Recoveries . . . 51
B.3 PFBS and Foam Conductivity . . . 52

List of Figures

1.1 Schematic overview of Foam Fractionation 2

2.1 PFAS Classification 5
2.2 Schematic structures of PFOS and PFOA, two common water-soluble PFAS, highlighting their amphiphilic structure with a hydrophobic fluorinated tail and a hydrophilic head group. . . 6
2.3 Schematic representation of osmosis and reverse osmosis across a semipermeable membrane. 7

3.1 Experimental Foam Fractionation Setup 15
3.2 Experimental timeline and sampling moments. 17

4.1 PFAS reporting by Dunea, converted to RO concentrate for a system with a removal efficiency of 80% [66]. 22
4.2 Mean relative concentrations of PFAS compounds measured in influent (n=3) and effluent (n=3) samples during the field blank test, expressed as a percentage of the total mean influent concentration. Error bars represent the relative minimum and maximum measured concentrations. 22
4.3 Foam layer during experiments. 24
4.4 Removal efficiency per experiment. 27
4.5 Enrichment factor per experiment. 27
4.6 Total mass balance percentages per experiment. 28
4.7 Summed PFAS concentrations relative to the total influent concentration of CT (set to 100%) grouped by compound class in the influent and effluent (A) and foamate (B) for each experiment. Bars represent mean relative concentrations, and error bars indicate the relative minimum and maximum measured values. 29
4.8 Compound-specific removal efficiencies. 30
4.9 Compound-specific enrichment factors. 31
4.10 PFOS concentrations in the influent, effluent and foamate relative to the CT influent concentration (set to 100%). (a) shows all experiments on a common relative scale using the compound-specific LOQ, while (b) shows the CT and BD30 experiments using a lower, batch-specific LOQ. The dashed lines indicate the LOQ and calibration limit. 32
4.11 PFOA concentrations in the influent, effluent and foamate relative to the CT influent concentration (set to 100%). (a) shows all experiments on a common relative scale using the compound-specific LOQ, while (b) shows the CT and BD30 experiments using a lower, batch-specific LOQ. The dashed lines indicate the LOQ and calibration limit. 32
4.12 Compound-specific mass balance recovery. 33

B.1 Compound-specific PFAS concentrations. The bars represent the mean measured concentrations, and the error bars indicate the minimum and maximum measured values. 47
B.2 Compound-specific PFAS concentrations. The bars represent the mean measured concentrations, and the error bars indicate the minimum and maximum measured values. 48
B.3 Compound-specific PFAS removal efficiencies for all experiments. The bars represent the mean removal efficiency, and the error bars indicate the minimum and maximum calculated removal efficiencies. 49

B.4 Compound-specific PFAS enrichment factors for all experiments. The bars represent the mean enrichment factor, and the error bars indicate the minimum and maximum calculated enrichment factors. 50
B.5 Compound-specific PFAS mass balance recoveries for all experiments. The bars represent the mean mass balance recovery, and the error bars indicate the minimum and maximum calculated mass balance recoveries. 51
B.6 Relationship between foam conductivity and mean PFBS concentration in the foamate. Each point represents one experimental condition. The relationship should be interpreted as exploratory, since conductivity was not varied as an independent experimental parameter. . . 52

List of Tables

2.1 Molecular weight of common PFAS [36][37] . . . 7
2.2 Saturation states . . . 8
2.3 Scale inhibiting mechanism per active ingredient [43] [46] . . . 10

3.1 Tested antiscalants . . . 14
3.2 Experiment IDs . . . 14
3.3 Operational Parameters . . . 16
3.4 Samples Analysed per Experiment. . . . 17
3.5 Calculated LOQs and lowest calibration concentrations for PFAS compounds with non-zero blank concentrations. . . . 18
3.6 Overview of experiments and samples included in analytical batch 1 and batch 2. . . . 19

4.1 Water quality parameters of RO concentrate measured at Het Waterlaboratorium. . . . 21
4.2 Relative differences between mean influent and effluent concentrations for each PFAS detected in the field blank. . . . 23
4.3 Measured viscosity and surface tension for all experiments. . . . 23
4.4 Average pH and conductivity measured during the experiments. . . . 25
4.5 Average influent flow and foam percentage for each experiment. . . . 26

A.1 All analysed PFAS grouped . . . 43
A.2 Blank averages, blank standard deviations and calculated LOQs for different PFAS . . . 44
A.3 Minimum calibration concentrations for the analysed PFAS compounds. . . . 45

B.1 Reported TOC concentrations for influent and effluent samples of the different experiments 46

1

Introduction

1.1. Background and Context

In 2015, the United Nations introduced the 2030 Agenda for Sustainable Development, containing 17 Sustainable Development Goals (SDGs) to promote efforts towards a more sustainable future. One of these, SDG 6, calls for universal access to safe and clean drinking water and sanitation for all people by 2030 [1]. While significant progress has been made worldwide, ensuring the quality and safety of drinking water remains a pressing and complex challenge.

One of the most significant, and increasingly urgent, threats to drinking water safety is the widespread contamination of water sources by per-and polyfluoroalkyl substances, more commonly known as PFAS. Since the last century, PFAS have been widely used due to their wide range of industrial and commercial applications, ranging from non-stick cookware and water-resistant textiles to food packaging, firefighting foams, and cosmetics [2]. What makes PFAS uniquely alarming is not only their widespread presence, but also their extremely persistent configuration: the high number carbon-fluorine bond, one of the strongest bonds in organic chemistry [3][4]. As a result, PFAS are commonly found in the environment, including in drinking water sources.

PFAS can enter the human body by various means, including through food, inhalation of aerosols, and drinking water [5]. Therefore, certain PFAS are commonly found in the human body, where they accumulate [6]. Research by the Dutch National Institute for Public Health and the Environment (RIVM) indicates that at least 25-50% of the Dutch population exceeds the human bio-monitoring limit value for the sum of various PFAS [7]. Excessive levels of PFAS in the body can affect the immune system, fertility, cholesterol levels and increase the risk of various types of cancer [8].

Growing awareness of PFAS contamination and its health risks has prompted stricter regulations. As of January 12, 2026, European Union member states are required to monitor PFAS levels in drinking water within the new limit values stated by the Drinking Water Directive. Based on this directive, the Netherlands has implemented a standard of 100 ng/l for the ”Sum of PFAS” in the Dutch Drinking Water Decree. This standard concerns the sum of PFAS that are considered a potential risk in connection with water intended for human consumption [9][10]. However, since 2022, the Dutch government has set a drinking water guideline value for PFAS of 4.4 ng/l, expressed as PFOA equivalents [11]. This guideline value is currently not legally binding but still poses challenges for drinking water companies in the Netherlands.

1.2. Problem Statement

Dunea is one of the ten drinking water companies in the Netherlands. The guideline value for PFAS of 4.4 ng/l is a relevant challenge. Dunea supplies drinking water to 1.4 million people in the west of South Holland. Between 2020 and 2024, they produced on average 80 billion litres of drinking water per year [12]. In order to produce such quantities while maintaining a high water quality, secure water sources and

a reliable treatment process are essential.

Dunea currently uses powdered activated carbon (PAC) as a PFAS removal step within their treatment system. PAC is able to remove 85% of the PFAS [13] through adsorption. A limitation is that, due to the short residence time of the PAC, its full adsorption capacity cannot be fully utilised. As a result, a significant fraction of the material remains unused, which represents an inefficient use of resources and leads to increased operational costs. Moreover, the environmental impact of PAC production can be substantial depending on the specific manufacturing processes. The incomplete utilisation of the material may also lead to unnecessary environmental burden. This issue is further amplified by the fact that PAC cannot be reactivated, meaning that all unused material ultimately becomes waste.

As well as advocating for a European ban on PFAS [13], Dunea is also conducting extensive research into alternative methods for removing PFAS from water. An example of this research is the UF-RO pilot. This pilot system consists of an ultra filtration (UF) system, followed by a reverse osmosis (RO) system. A recent study reviewing developments in membrane treatment technologies for PFAS removal shows an average PFAS removal efficiency of 98% using RO membranes [14]. However, this method presents a notable challenge: the generation of a concentrate stream (RO concentrate) in which PFAS concentrations are approximately five times higher compared to the raw water. Treating RO concentrate is essential to prevent shifting the contamination problem by ensuring that contaminants removed from the treated water are not simply discharged elsewhere, where they could cause environmental pollution.

1.3. Positioning

A promising concentrate treatment technique for PFAS removal is foam fractionation, which makes use of the affinity of surface-active compounds for the air-water interface. In foam fractionation, air bubbles are continuously introduced at the bottom of a column, filled with water or operated in a continuous-flow configuration. As bubbles rise through the water, surface-active compounds adsorb at the air-water interface and are carried upward with the foam. The foam is then collected and collapsed into a small, highly concentrated volume called the foamate, while the treated water exits as retentate [15]. A useful property of most PFAS is their ability to lower surface tension due to their amphiphilic nature [16], causing them to accumulate at the air-water interface due to the rising bubbles. Foam fractionation is particularly suitable for water matrices with higher PFAS concentrations [17], making it suitable for treatment of RO concentrate.

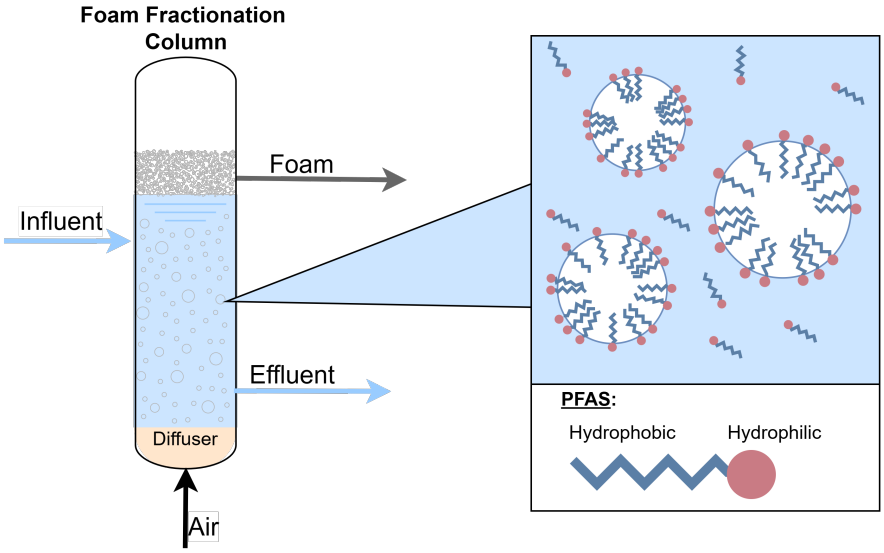

Figure 1.1: Schematic overview of Foam Fractionation

Research by McCleaf et al. [17] has shown that foam fractionation is an effective method for PFAS removal from nanofiltration (NF) concentrate and even found a higher PFAS removal efficiency compared to the removal efficiency in comparable studies investigating foam fractionation for treating landfill leachate. The authors suggest that the better removal efficiency may be due to the polymer antiscalant in the NF concentrate, which could increase the hydrophobicity of the PFAS molecules through charge interactions between the polymer and the PFAS molecule.

Since RO concentrates not only PFAS but also other dissolved compounds such as membrane antiscalants and natural organic matter (NOM), these co-concentrated substances may influence the performance of foam fractionation. Membrane antiscalants are added to membrane systems to disrupt scale formation within membranes to preserve membrane efficiency. Scaling occurs when dissolved ions in the feed water reach a state of local supersaturation: as water permeates through the membrane, most ions are retained, causing their concentration to increase near the membrane surface. The ion product (IP) exceeds its solubility product (K_{SP}), causing crystallization on the membrane surface, forming a scale [18]. Adding an antiscalant increases the solubility limits of the scaling salts. Antiscalants are predominantly made of polyelectrolytes, making them a type of polymer [19]. Antiscalants are retained on the concentrate side of the membrane and are therefore present in the concentrate stream.

The potential interaction between PFAS and antiscalants that may enhance PFAS removal efficiency of foam fraction, might be explained by the behaviour of weakly interacting polymer-surfactant systems. Petkova et al. [20] found that when polymer and surfactant carry the same charge, such systems demonstrate enhanced foam formation, foaminess and foam stability compared to surfactant solutions without polymers. This enhancement occurs because surfactant molecules first adsorb rapidly at the bubble surface, creating surface tension gradients that slow down foam film thinning. This gives the polymer time to also adsorb at the bubble surface, where it physically blocks the foam films from collapsing.

As most PFAS are anionic and surface-active compounds and antiscalants such as polycarboxylates and phosphonates are also anionic, interactions between the two during foam fractionation are plausible. However, no study to date has systematically investigated if these interactions exist and influence foam fractionation efficiency. This represents a research gap that this study aims to address.

1.4. Research Question and Objectives

Based on the expectation that PFAS-antiscalant interactions occur and building on the research gap identified in section 1.3, the objectives of this research are to systematically evaluate the performance of foam fractionation used on RO concentrate, and to determine whether different antiscalant types influence the PFAS removal efficiency of this process. Additionally, this study aims to investigate how antiscalants affect underlying mechanisms of foam fractionation. To address these objectives, the following research question has been formulated:

How do different antiscalants influence the performance and mechanisms of foam fractionation for the removal of PFAS from reverse osmosis concentrate from drinking water treatment?

To systematically answer this research question, the following sub-questions are formulated:

1. Do different antiscalants influence foam formation and foam characteristics?
2. Do different antiscalants influence the PFAS removal efficiency and enrichment factor during foam fractionation?
3. How can the influence of the tested antiscalants on the PFAS foam fractionation performance be explained?

2

Theoretical Background

2.1. Per- and Polyfluoroalkyl Substances (PFAS)

Per- and polyfluoroalkyl substances (PFAS), as stated previously, are a group of human-made substances that have been widely used in industrial applications and consumer products for decades. The estimated number of chemicals in the PFAS family varies widely depending on the source, with figures ranging from 4,000 to 12,000 distinct compounds [3][21][22]. PFAS are highly fluorinated aliphatic substances in which one or more carbon (C) atoms, of which all hydrogen (H) atoms are replaced by fluorine (F) atoms, giving the perfluoroalkyl moiety ($C_nF_{2n+1}-$) [4]. Well-known examples such as PFOA, PFOS and GenX have been linked to environmental and health-related concerns [23].

2.1.1. Classification

PFAS form a large and diverse group of substances with a wide range of physicochemical properties [24]. Some common PFAS classifications are based on their polymerisation state, fluorination state, and chain length. Based on their polymerisation state, PFAS can be divided into two primary classes: polymeric and non-polymeric. Polymers are large molecules formed by combining many identical smaller molecules, known as monomers [25]. As shown in figure 2.1, there are three types of polymeric PFAS. An example is polytetrafluoroethylene (PTFE), more commonly known as Teflon [26]. Although polymeric PFAS are, strictly speaking, not water-soluble and therefore fall outside the scope of this research, they are closely related to non-polymeric PFAS. Non-polymeric PFAS are used as processing aids in the production of certain fluoropolymers, such as Teflon. Research has shown that fluoropolymer production plants emit PFAS into the air and surrounding surface waters [27]. In addition, studies have shown that certain polymeric PFAS can gradually degrade in soil and water, resulting in the continued release of non-polymeric PFAS [28].

Non-polymeric PFAS can be divided into two subclasses by their fluorination state: **per**fluoroalkyl substances and **poly**fluoroalkyl substances. In **per**fluoroalkyl substances fluorines have replaced all hydrogens on all alkyl carbon atoms. For **poly**fluoroalkyl substances, all hydrogens on at least one (but not all) alkyl carbon atoms have been replaced by fluorines [4]. These two subclasses include many groups, sub-groups and compounds of which some are shown in figure 2.1.

$C_nF_{2n+1}-R$ is a common general formula for many PFAS, especially from the perfluoroalkyl acids group (PFAAs). "R" represents the functional head group, often being carboxylic acid (PFCAs), sulphonic acid (PFSAs) or phosphoric acid (PFPAs) [29]. For PFCAs, PFSAs and their precursors a distinction between long-chain and short-chain is made. Where long-chain refers to [4][25]:

- PFCAs: seven or more perfluorinated carbons ($C_nF_{2n+1}COOH$, n $\geq$ 7)
- PFSAs: six or more perfluorinated carbons ($C_nF_{2n+1}SO_3H$, n $\geq$ 6)

And short-chain refers to [4][25]:

- PFCAs: less than seven perfluorinated carbons ($C_nF_{2n+1}COOH$, n < 7)
- PFSAs: less than six perfluorinated carbons ($C_nF_{2n+1}SO_3H$, n < 6)

Although other perfluoroalkyl substances are not included within this classification, Buck et al. [4] states that a perfluoroalkyl chain with seven or more carbon atoms may be considered "long-chain". Table A.1 shows all analysed PFAS grouped.

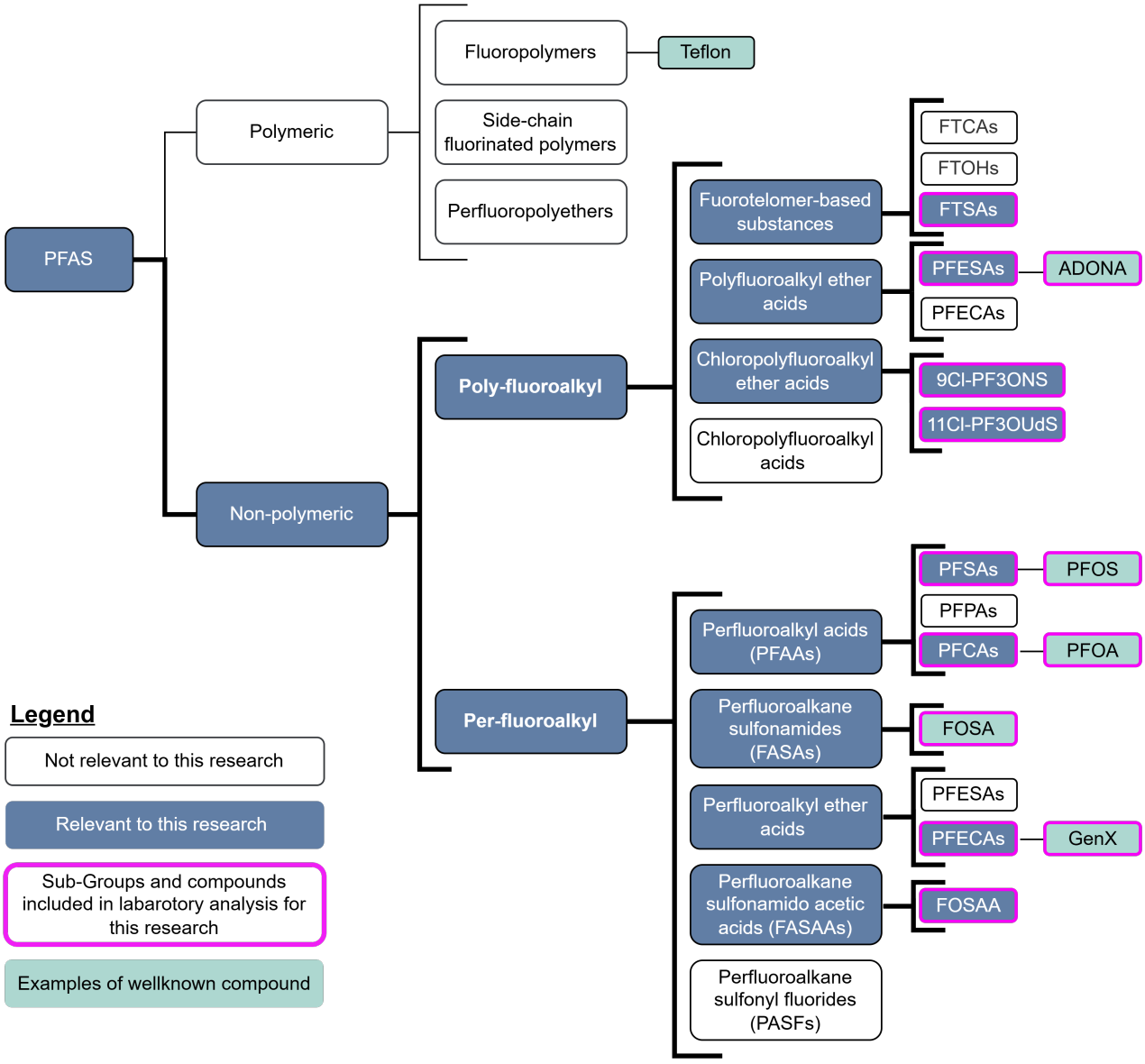

Figure 2.1: PFAS Classification

2.1.2. Surface Activity and Amphiphilic Structure of PFAS

For this research, water-soluble and amphiphilic PFAS are particularly relevant, as these compounds can interact with both the aqueous phase and air-water interfaces. Common examples include PFOS and PFOA, whose molecular structures are shown in figure 2.2. Both compounds contain a hydrophobic fluorinated tail and a hydrophilic head group. This amphiphilic structure allows the molecules to orient at the air-water interface, with the hydrophilic head group remaining associated with water and the hydrophobic tail pointing away from the aqueous phase [25][30].

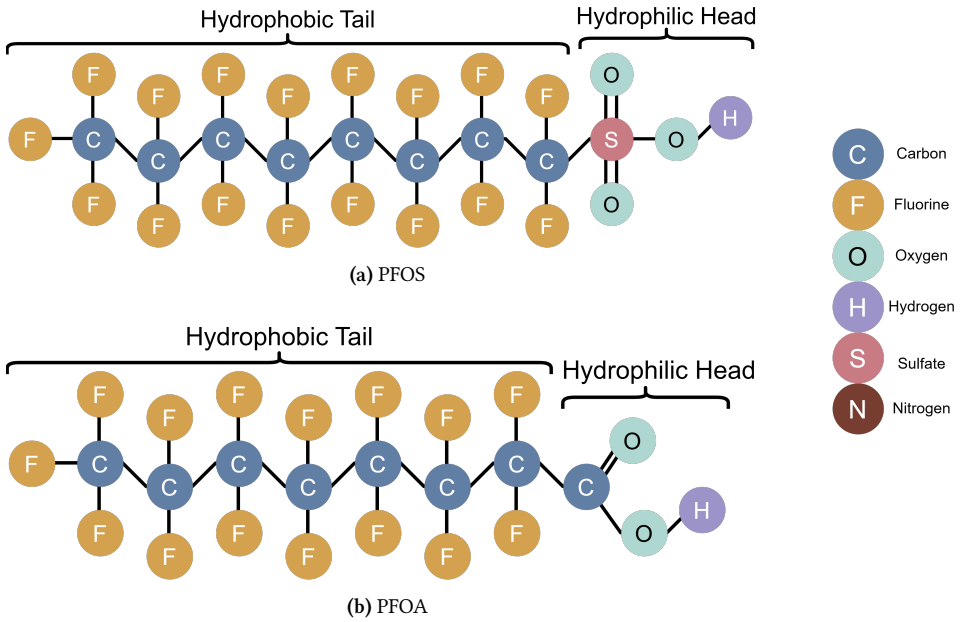

(a) PFOS

(b) PFOA

Figure 2.2: Schematic structures of PFOS and PFOA, two common water-soluble PFAS, highlighting their amphiphilic structure with a hydrophobic fluorinated tail and a hydrophilic head group.

Long-chain PFAS, such as PFOA and PFOS, generally have a stronger hydrophobic character and a greater tendency to partition to interfaces than short-chain PFAS. This is due to their longer fluorinated tail, which increases their hydrophobicity. In contrast, shorter-chain PFAS are more water-soluble and generally less surface-active compared to long-chain PFAS such as PFOS and PFOA [4][30].

2.2. Reverse Osmosis as a PFAS Treatment Technology

Dunea is currently operating a pilot-scale treatment train consisting of an ultrafiltration (UF) unit, which removes suspended solids and colloidal material, followed by a reverse osmosis (RO) unit that rejects dissolved salts and organic micropollutants such as PFAS. Since this research focusses on RO concentrate, UF is not discussed in further detail but the focus of this section will be on the RO process.

2.2.1. Principle of Reverse Osmosis

Reverse osmosis (RO) is a membrane filtration process used to remove salts and organic micropollutants from water. To understand how it works, it helps to first understand osmosis, the natural process it utilises.

Osmosis is the process by which water migrates through a semipermeable membrane from a region of lower solute concentration to a region of higher solute concentration. This movement is driven by the osmotic pressure difference across the membrane: the greater the concentration difference, the stronger the driving force.

In reverse osmosis, this natural flow is deliberately reversed. By applying an external pressure exceeding the osmotic pressure of the feed water, water molecules are forced through the semipermeable membrane against their natural direction of flow, from the concentrated side to the dilute side. Because the dissolved solutes cannot pass through the membrane, they are effectively retained and separated from the permeating water [31][18]. Figure 2.3 illustrates the principle of this process.

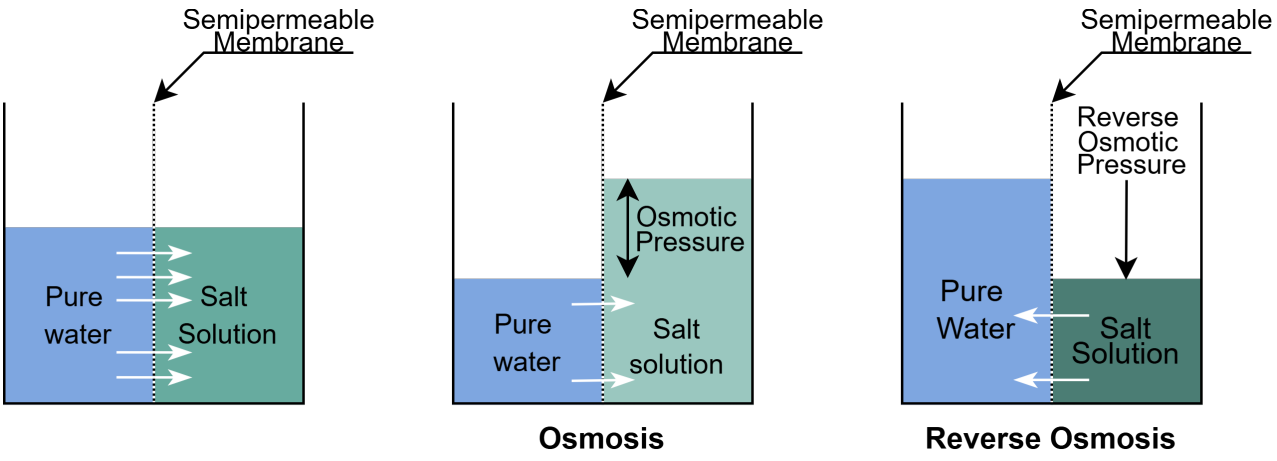

Figure 2.3: Schematic representation of osmosis and reverse osmosis across a semipermeable membrane.

2.2.2. Reverse Osmosis Membranes

Different types of RO membrane configurations are available but the most common type is a spiral wound membrane. This is also the RO membrane configuration used at Dunea's UF/RO pilot. A spiral wound RO membrane usually consists of several sheets of semipermeable membrane, feed spacer and permeate spacer material glued together to form envelope-shaped layers. The layers are tightly wound around a central permeate collection pipe, through which the filtered water (permeate) is transported. The spiral configuration allows a large membrane surface to fit inside a compact module [32][33]. The influent, also called the feed flow, enters the membrane under high pressure and is separated by the membrane into two flows: a pure water stream called the permeate flow and a concentrated solute stream called the concentrate (or retentate) flow. RO modules are always operated in cross-flow operation. This means that per membrane element only around 10% of the flow is produced as permeate. For this reason membrane elements are placed in series to achieve higher recovery [31]. By placing multiple membrane elements in series, Dunea's pilot system operates at an overall recovery of 80%, while the remaining 20% ends up as concentrate.

2.2.3. PFAS Removal and Co-concentrates

In RO membranes, size exclusion is the main removal mechanism. RO membranes have a molecular weight cut-off (MWCO) ranging from 20 - 200 Da, commonly falling below 100 Da [34][35]. This means that RO is highly effective for separating substances with a molecular weight higher than the MWCO, as these cannot pass through the membrane. As the molecular weight of water-soluble PFAS ranges between from 114 Da (TFA) to approximately 750 Da, RO is an effective method. Table 2.1 shows the molecular weight of some common PFAS.

	TFA	GenX	PFOA	PFOS
Molecular Weight [Da]	114.02	330.05	414.07	500.13

Table 2.1: Molecular weight of common PFAS [36][37]

2.2.4. Membrane Failure Mechanisms

RO membranes are also highly susceptible to performance decline and even failure. This can occur due to chemical degradation, mechanical damage, or, most commonly, fouling and scaling. Fouling refers to the accumulation of unwanted material on the membrane surface or within its pores. A particularly problematic form is biofouling, which occurs when microorganisms adhere to the membrane surface and develop into

a biofilm. Once established, the biofilm traps additional organic matter and particles, increasing hydraulic resistance and reducing permeability [38][18].

Biofouling is generally considered the most frequent and persistent challenge in RO systems, and it can worsen other failure mechanisms, such as scaling and organic fouling. To mitigate biofouling, appropriate pretreatment steps (like UF), regular cleaning protocols, and optimised operational conditions (such as maintaining adequate cross-flow velocity and minimising nutrient availability) are essential.

Although scale deposits can contribute to fouling when crystalline particles are already present in the RO feed, the term "scaling" specifically refers to the precipitation of dissolved solutes as their concentration increases beyond saturation [18]. Because RO membranes also reject dissolved ions, these accumulate in the concentrate stream. As water flows through the membrane while solutes, ions and salts stay behind, their local concentration rises, which increases the likelihood that saturation conditions are exceeded and scaling occurs.

To determine whether a compound is saturated, undersaturated or supersaturated the solubility product (K_{SP}) can be used. The K_{SP} is an equilibrium constant that represents the maximum product of ion concentrations that can exist in solution at equilibrium before precipitation occurs [39][40]. It is defined for the dissolution reaction shown in equation (2.1) and expressed mathematically in equation (2.2).

$$A_m B_n(s) \leftrightarrow mA_{(aq)} + nB_{(aq)} \tag{2.1}$$

$$K_{SP} = [A]^m [B]^n \tag{2.2}$$

In contrast to K_{SP}, which is a fixed constant at a given temperature, the ion product (IP) is calculated using the actual measured ion concentrations at any given moment [41]:

$$IP = [A]^m [B]^n \tag{2.3}$$

By comparing the IP with the K_{SP}, the saturation state can be determined as shown in table 2.2.

IP < K_{SP}	Undersaturated	More can dissolve
IP = K_{SP}	Saturated	Equilibrium
IP > K_{SP}	Supersaturated	Precipitation might occur

Table 2.2: Saturation states

If a solution exceeds a critical supersaturation level, crystallisation and with this, the formation of scale begins. This process follows a few steps, starting with ion clustering as proto-nuclei consisting of up to 1000 atoms. These proto-nuclei grow into bigger more ordered structures called nuclei which eventually form crystals [42]. This process can be affected by various factors and methods. One of these methods is the use of an antiscalant and will be further discussed in section 2.3.

2.3. Membrane Antiscalants

There are various methods for preventing or delaying membrane failure. Some methods for combating (bio)fouling have already been mentioned in section 2.2.4 but as this is not the focus of this study, they will not be further discussed. However, this study does focus on antiscalants, a widely used method for scaling prevention. This section explores in more detail how antiscalants work, what their typical active ingredients are, and how these might influence foaming.

2.3.1. Scale Inhibiting Mechanisms

Antiscalants interfere with one or more of the crystallisation stages mentioned in section 2.2.4. So, in general, antiscalants do not remove the scale forming molecules, but postpone the initiation of crystallisation or slow down crystal growth. There are four main scale inhibiting mechanisms which are used in antiscalants: threshold inhibition, crystal modification, dispersion, and chelating [43][42][44][45].

- **Threshold inhibition**: Threshold inhibition is the ability of antiscalants to prevent crystal formation at the proto-nuclei formation phase in a supersaturated solution. By adsorbing onto newly formed submicroscopic nuclei, their negatively charged groups disturb the ionic balance required for crystal growth, delaying precipitation. This mechanism effectively slows down the start of scaling even at low antiscalant concentrations.
- **Crystal modification**: Crystal modification occurs when antiscalants bind to active growth sites on forming crystals and disrupt the arrangement of the crystal structure. This leads to distorted, non-adherent, weaker shaped crystals, making them less likely to accumulate on surfaces.
- **Dispersion**: Dispersion refers to the ability of antiscalants to adsorb onto scale particles and impart additional negative charge, increasing electrostatic repulsion. This prevents particles from aggregating and keeps them suspended in solution, stopping further crystal growth.
- **Chelating**: Chelating agents work by forming water-soluble complexes by binding cations thereby removing these ions from participating in scale-forming reactions. Though chelating agents are not commonly used in RO systems as high concentrations of chemical are needed for successful scale inhibition.

2.3.2. Typical active ingredients of antiscalant

The exact formulation of commercial antiscalants is often not disclosed by manufacturers. This makes it difficult to determine which active ingredients are present in a specific product. However, based on literature, the most common active ingredients can be grouped according to their chemical structure and functional groups. In this section, three groups are discussed: phosphate and phosphonate-based, polycarboxylates, and biobased [39]. These groups are not always completely separate, since some commercial products combine multiple functional groups, but the classification is useful for understanding their expected scale inhibition mechanisms and possible relevance for foam formation or PFAS interactions.

Phosphate and Phosphonate-based

Phosphorus-based antiscalants represent the largest share of global antiscalant use and are divided into phosphate- and phosphonate-based compounds. Phosphates, built around the orthophosphate ion PO_4^{3-}, have been used to inhibit scale formation but are prone to hydrolysis into orthophosphate, which can promote biofouling by acting as a nutrient source. Phosphonates contain a more stable carbon–phosphorus (C–P) bond, giving them greater resistance to hydrolysis and broader applicability [43] [46]. Both groups primarily act through threshold inhibition and crystal distortion, adsorbing onto crystal nuclei at substoichiometric concentrations to block further growth. Their main drawback is the risk of phosphorus-driven eutrophication and biofouling.

Polycarboxylates

Stricter phosphorus discharge regulations have driven interest in phosphorus-free polycarboxylate antiscalants, such as polyacrylic acid (PAA), polymaleic acid, and their copolymers. These polymers carry multiple carboxylic acid groups that chelate scale-forming cations and adsorb onto crystal surfaces, inhibiting growth through crystal distortion and dispersion. Copolymers combining several functional groups generally outperform single-function homopolymers due to multiple simultaneous inhibition mechanisms [43] [46].

Biobased antiscalants

Biobased antiscalants, derived from renewable sources, include compounds such as carboxymethyl cellulose, carboxymethyl inulin, polyaspartic acid, and chitosan derivatives. They rely on similar mechanisms to synthetic polycarboxylates but have the benefit of biodegradability and low toxicity, although they sometimes require higher dosages to achieve comparable performance [43] [46].

Antiscalant Class	Primary Mechanisms
Phosphates and phosphonates	Threshold inhibition, crystal growth inhibition
Polycarboxylates	Crystal growth inhibition, dispersion
Bio-based antiscalants	Crystal growth inhibition, dispersion

Table 2.3: Scale inhibiting mechanism per active ingredient [43] [46]

2.4. Foam Fractionation

Foam fractionation (FF) is a separation method that exploits the amphiphilic nature of certain dissolved compounds to adsorb onto bubble surfaces. Amphiphilic molecules, including surface-active agents (surfactants), possess both a hydrophilic (polar, "water-loving") and hydrophobic (non-polar, "water-fearing") part, enabling them to adsorb at the air-water interface when gas bubbles are introduced [47][48]. This property is utilised in FF by introducing small bubbles into the water, creating a large number of available bubble surfaces. Surfactants are adsorbed to these available surfaces and accumulate at the air-water interface, creating a surfactant-rich foam [15].

2.4.1. Foam Affecting Factors

Foam can be defined as a dispersed gas-liquid system in which gas bubbles are separated by thin liquid films, also referred to as lamellae. Since bubbles are thermodynamically unstable, foam stability is mainly a kinetic property: the foam does not remain stable indefinitely, but its collapse can be delayed by surface-active compounds and other stabilising additives [49][50]. In foam-based separation processes, such as foam fractionation, both foamability and foam stability are important. Foamability describes the ability of a liquid to generate foam, whereas foam stability describes how the foam changes over time [51].

Foam Formation and Stabilisation

Foam formation occurs when gas is introduced into a bulk liquid, for example by sparging, shaking or another mechanical foaming method. This creates new gas-liquid interfacial area, which requires energy because of the interfacial tension of the liquid [52]. Surface-active compounds, such as surfactants, adsorb at this newly formed interface and reduce the interfacial tension. This lowers the energy required for bubble formation and allows bubbles to be generated more easily. In addition, adsorbed surfactants can form a viscoelastic interfacial layer around the bubbles, which increases the resistance of the liquid film against rupture and slows down coalescence [53][49].

Foam Structure and Destabilising Mechanisms

After foam is formed, it evolves over time through several destabilisation mechanisms. One important mechanism is gravitational drainage. Liquid drains from the lamellae and plateau borders influenced by gravity and capillary forces, causing thinning of the liquid films between bubbles. As a result, the films become more vulnerable to collapse [49][51]. Drainage can be slowed by increasing the bulk viscosity of the liquid or by increasing the interfacial viscosity through additives such as polymers, co-surfactants or particles [51][50].

A second mechanism is coalescence, in which two neighbouring bubbles merge into one bubble after the liquid film between them collapse. Coalescence reduces the number of bubbles and increases the average bubble size, which generally decreases foam stability [49].

A third mechanism is Ostwald ripening. Because the internal pressure of small bubbles is higher than that of larger bubbles, gas can diffuse from small bubbles to larger bubbles through the liquid films and is called bubble coarsening. This causes small bubbles to shrink and large bubbles to grow, increasing the average bubble size and eventually weakening the foam structure [49][50]. Smaller and more spherical bubbles are generally more stable because they have a more uniform interfacial tension distribution, thicker liquid films and a denser packing structure, whereas larger bubbles tend to drain faster and are more prone to collapse [50].

Influence of Liquid Composition

The composition of the bulk liquid strongly influences both foamability and foam stability. Surfactant type and concentration determine the stability of the gas-liquid interface. Increasing surfactant concentration can improve foamability and foam stability up to a certain concentration, after which further addition generally results in little to no additional improvement. The gas-liquid interface is already effectively saturated. [54][49].

The type of surfactant is also important as it strongly affects foam stability. Ionic surfactants can stabilise foam films through electrostatic repulsion, the bubble surfaces are charged and repel each other, thereby reducing bubble coalescence. While non-ionic surfactants mainly stabilise films through steric and interfacial effects. Salinity and pH are especially important for ionic surfactants, because they can change surfactant adsorption and the strength of repulsive forces in the liquid film [50]. Salinity can improve foam stability at moderate levels by improving surfactant adsorption to the interface, but too much salt can reduce film stability and promote coalescence [51][50].

Polymers can improve foam stability by increasing the viscosity of the bulk liquid, slowing drainage and strengthening the films between bubbles [50]. However, this effect strongly depends on polymer concentration. Kedir et al. [51] showed that polymer addition improved foamability and stability below a certain concentration, but could boost antifoaming above this concentration.

Nanoparticles can also stabilise foams by adsorbing at the gas-liquid interface and forming a protective layer around bubbles. This can strengthen the interfacial film and reduce coalescence. However, at too high concentrations, nanoparticles may aggregate and reduce foam stability instead of improving it [50][49].

Influence of Operational Conditions

Operational conditions such as gas flow rate, gas-to-liquid ratio, temperature and pressure also influence foam behaviour. Gas flow rate affects the number of bubbles formed, the available bubble interfaces and the residence time of bubbles in the liquid. Temperature can reduce stability by accelerating drainage, increasing gas diffusion and changing surfactant adsorption behaviour. Pressure can also affect foam stability by changing gas density, bubble size and interfacial properties [50][49].

For foam fractionation, the most desirable foam is not necessarily the most stable foam. Foam fractionation is based on the selective adsorption of surface-active compounds at rising bubble surfaces; the foam that forms at the top of the liquid is enriched in the adsorbed compounds and can be collected as foamate [54]. Some drainage is beneficial because excess liquid and less surface-active compounds can drain back into the bulk phase, increasing enrichment in the collected foam [53]. Therefore, the optimal foam for foam fractionation should be stable enough to transport surface-active compounds upward, but not so wet or persistent that it carries excessive liquid and reduces separation efficiency.

2.4.2. Possible Influence on FF and PFAS Removal

Antiscalants may influence foam fractionation and PFAS removal through several indirect mechanisms. Foam fractionation depends on the adsorption of surface-active PFAS at the air-water interface. Therefore, changes in water chemistry, interfacial properties or foam stability may affect the transfer of PFAS from the bulk liquid to the foam phase. Antiscalants are usually organic compounds and many contain charged

functional groups, such as carboxylate, phosphonate or sulphonate groups [43][46]. These groups allow antiscalants to interact with scale-forming ions, but they may also influence the water matrix during foam fractionation.

The effect of antiscalants on foam fractionation can be either positive or negative. They might influence pH, salinity or ionic strength, and by this influence electrostatic interactions and PFAS adsorption at the air-water interface [55][56]. Polymeric antiscalants may also affect foam film stability, liquid drainage, or compete with PFAS for adsorption sites at the air-water interface. Literature on polymer-surfactant systems shows that polymers can either improve or reduce foamability and foam stability, depending on their charge, concentration and the water matrix [20][51].

For foam fractionation, the most desirable foam is not necessarily the most stable foam. Foam fractionation is based on the selective adsorption of surface-active compounds at rising bubble surfaces. The foam that forms at the top of the liquid is enriched in the adsorbed compounds and can be collected as foamate [54]. Some drainage is beneficial because excess liquid and less surface-active compounds can drain back into the bulk phase, increasing enrichment in the collected foam [53]. Therefore, antiscalants could improve PFAS removal if they promote sufficient foam formation and PFAS transport, but they could also reduce performance if they compete with PFAS at the interface, destabilise the foam, or create foam that is too wet and carries excessive bulk liquid.

3

Methodology

This study aims to investigate the effects of different antiscalants on foam fractionation as a treatment step for treating reverse osmosis concentrate. This chapter provides a detailed description of the experimental setup, operating conditions, and materials used, including water matrix, antiscalants, and experimental procedures.

3.1. Concentrate Stream

For all experiments, the same concentrate stream from Dunea's UF/RO pilot was used. The UF/RO pilot system is used to treat aerobic surface water. All water used for the experiments was collected on a single day and in a single batch to ensure that the water matrix remained as stable as possible throughout the experiments, thereby minimising variation in water composition between individual experiments. To obtain a concentrate stream without antiscalant concentrations, the antiscalant dosing to the RO system was temporarily switched off one hour prior to water collection. During water collection, the RO system was operated at a recovery rate of 80%. The concentrate was stored in the fridge in the Waterlab in 10-L jerrycans that had previously been used only for demineralised water.

3.2. Antiscalants

Table 3.1 lists the antiscalants that will be used in this study. As stated before, antiscalant manufacturers generally provide limited information regarding the exact composition of their products. The specific active ingredients are often not fully disclosed, nor are their concentrations, and information on other components in the formulations is typically unavailable. The table therefore includes only the information that could be obtained from publicly available sources.

Antiscalant	Active ingredient	Scale Prevention Mechanism	Target Scalant
4Aqua OSM BD30	Carboxymethyl inulin	Threshold inhibitor	$CaCO_3$, $CaSO_4$, $BaSO_4$, $SrSO_4$
Vitec 1141	Phosphonic and polycarboxylic acids	Dispersion and threshold inhibitor	Inorganic deposits
Aquatreat 535	Polymers (phosphate and phosphonate free)		Organic and inorganic deposits
Sokalan RO400	Polycarboxylic acid	Inhibition and dispersion	$CaCO_3$, $CaSO_4$, $BaSO_4$
Ameroyal 363	Polymer-based/ Polyacrylates	Inhibition	$CaCO_3$, $CaSO_4$, $BaSO_4$, $SrSO_4$
Vitec 1200	Polycarboxylic acid	Inhibition and dispersion	$CaCO_3$, $CaSO_4$, $BaSO_4$, $SrSO_4$, SiO_2. CaF

Compiled by author [57][58][59][60][61][62][63]

Table 3.1: Tested antiscalants

Throughout the remainder of this thesis, each experiment was assigned a unique experiment ID. These IDs are used consistently in figures, tables and text and are shown in table 3.2.

Experiment ID	Influent Composition
CT	RO concentrate
BD30	RO concentrate + 4Aqua OSM BD30
V1141	RO concentrate + Vitec 1141
AQUA	RO concentrate + Aquatreat 535
RO400	RO concentrate + Sokalan RO400
AM363	RO concentrate + Ameroyal 363
V1200	RO concentrate + Vitec 1200

Table 3.2: Experiment IDs

3.2.1. Antiscalant Dosing

The antiscalant concentration used in all antiscalant-containing experiments was based on the dosage of 4Aqua OSM BD30 used by Dunea. In the pilot system this antiscalant is dosed with a concentration of 4.7 mg/L (ppm) in the feed water. Since the RO system operates at a recovery of approximately 80%, the antiscalant concentration in the concentrate stream is expected to increase by a factor of five, resulting in an estimated concentration of 23.5 mg/L.

This concentration was used in all antiscalant-containing experiments to ensure that the laboratory conditions closely represented the actual operating conditions of the full-scale installation. Although antiscalant suppliers generally determine the required dosage using software based on the specific water matrix, the details of these calculations are typically not disclosed. Access to such software was not available during this study. Furthermore, the concentrations of the active ingredients in the various antiscalants are usually unknown. This makes it difficult to determine an antiscalant concentration that is representative for

the various antiscalants. For this reason, the concentration used by Dunea was assumed to be the most representative value.

3.3. Experimental Setup and Approach

3.3.1. Experimental Setup Description

Figure 3.1 shows a schematic overview of the experimental setup. The setup consisted of a PVC cylindrical column with an inner diameter of 8 cm and a height of 100 cm. Along the entire length of the column, valves with a diameter of 8 mm were positioned at 10 cm intervals. The first valve was located 10 cm from the bottom of the column and served as the effluent outlet. The valve at 40 cm was used for influent, while a valve at 50 cm was connected to the foam collection vessel, which was maintained under low pressure using a vacuum pump. The top of the column was closed during operation.

Influent was supplied to the column using a peristaltic pump. To maintain a constant water level within the column, a standpipe was installed downstream of the effluent outlet. The standpipe could be adjusted vertically by sliding it up or down the column.

Air was introduced at the bottom of the column through a porous glass frit with P4 porosity (pore size range of: 10-16 µm). A rotameter was placed upstream of the air supply to monitor and regulate the airflow. The air supply was provided via 10 mm tubes, while all other tubing had a diameter of 15 mm.

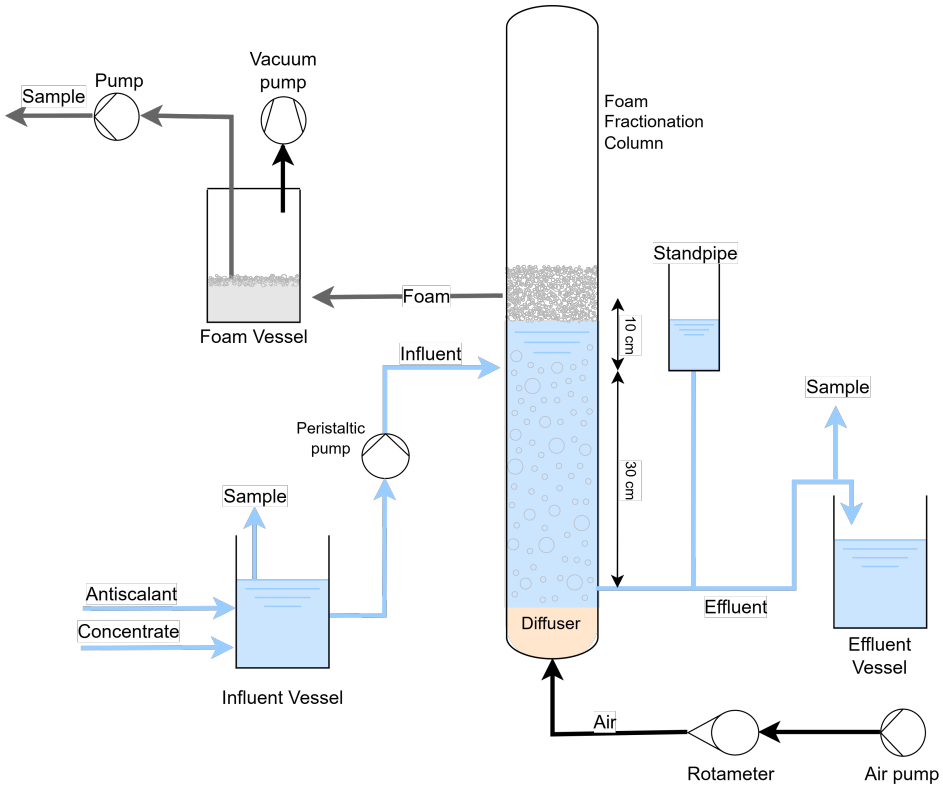

Figure 3.1: Experimental Foam Fractionation Setup

3.3.2. Experimental Parameters

Table 3.3 shows operational conditions and parameters that were established. How this was done is further explained in section 3.3.3. The operating water level inside the column was controlled using the standpipe connected to the effluent outlet and was set at 45 cm, about 3 cm below the foam outlet, resulting in a liquid volume (V_{liquid}) of 2.35 L in the column. The positions of the influent inlet (40 cm) and effluent outlet

(10 cm) were kept constant throughout all experiments. Airflow (Q_{air}) was regulated using a rotameter and maintained at 4 L/min during operation. The target foam percentage ($foam_{\%}$) was 20%. The peristaltic pump was calibrated to result in an influent flow (Q_{in}) of approximately 82 mL/min. This resulted in a pump speed between 36 and 40 RPM. The contact time (t_c) was therefore approximately 30 minutes (equation (3.1)).

Parameter	Variable
t_c	30 min
V_{liquid}	2.35 L
Q_{in}	82 ml/min
Q_{air}	4 l/min
$foam_{\%}$	20%

Table 3.3: Operational Parameters

$$t_c = \frac{V_{column}}{Q_{in}} \tag{3.1}$$

3.3.3. Experimental Procedure

Prior to all experiments, the effective water volume was determined experimentally by filling the column to the operating water level and measuring the required volume, resulting in approximately 2.35 l. After this the liquid flow rate of the peristaltic pump was estimated by operating the pump at different rotational speeds (RPM) and measuring the time required to fill a container. The container was weighed before and after a fixed time interval to determine the pumped volume and corresponding flow rate. Based on these preliminary tests, the target pump setting was narrowed down to approximately 36 and 39 RPM. As the actual flow is not only dependent on the pump speed but is also influenced by the pressure in the column and the state of the tubes, the pump speed had to be calibrated prior to each experiment to give an average liquid flow rate of 82 mL/min.

A field blank test was conducted to verify that the column and experimental setup were free from PFAS contamination and that adsorption to the column walls was negligible. During the field blank test, the concentrate was pumped from the influent through the column to the effluent, while the airflow and foamate collection were switched off. After contact times of 30 minutes, three influent and three effluent samples were collected for PFAS testing.

Following the field blank test, the column experiments were conducted.

3.4. Sampling

The experimental timeline is shown in figure 3.2. All experiments were conducted under continuous operation for a total duration of four contact times. Samples were taken after two, three and four contact times instead of performing experimental triplicates. For this, steady-state operation was required, as stated in a study by McCleaf et al. [64]. This study indicated that PFAS removal using continuous foam fractionation remained stable after the first contact time had been reached. This was confirmed by Smith et al. [65]. However, for certainty, the first set of samples was taken after two contact times had passed. Samples were taken from the influent, effluent and foamate.

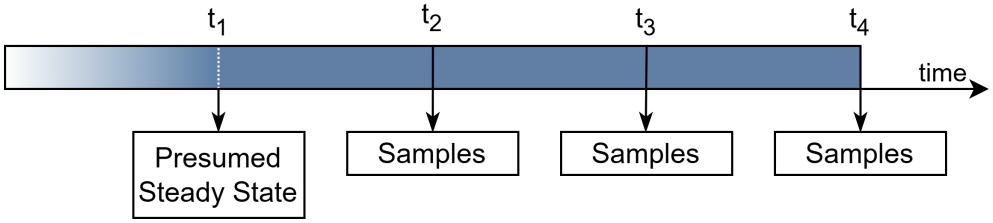

Figure 3.2: Experimental timeline and sampling moments.

Table 3.4 shows the samples that were taken for each experiment. Figure 3.1 shows where samples were collected. Depending on the sampling location, samples were either collected directly from the outlet stream into the tubes or via a dedicated sampling valve installed at the sampling point. Influent samples were collected from the bulk influent, whereas effluent and foamate samples were collected from their designated sampling tubes. Samples taken for PFAS analysis were collected into 15 mL forensic DNA grade Eppendorf conical tubes, to minimise the risk of PFAS contamination, and remained in these during storage until sample preparation. TOC samples were collected into 50 mL tubes and stored and acidified the same day. General samples were collected in 30 mL tubes and were disposed of after measurement. In total, 63 PFAS, 42 TOC and 63 general samples were taken. Based on the assumption that the influent matrix stayed constant for the duration of each individual experiment, only one of the PFAS influent samples and one of the TOC influent samples were analysed per experiment.

Stream	PFAS	TOC	General[1]
Influent	15 mL	35 mL	20 mL
Effluent	15 mL	35 mL	20 mL
Foamate	15 mL	-	20 mL

[1] General samples are used for measuring pH, conductivity and temperature using a sensor

Table 3.4: Samples Analysed per Experiment.

As shown in figure 3.1, the foam vessel is vacuum-sealed. For this reason, the collapsed foam, foamate, was pumped into another vessel for sampling. Once steady-state conditions had been reached, the vessel was emptied and foamate samples were taken from it. As the influent was assumed to remain stable throughout each experiment, only one sample was analysed per experiment. Three influent samples were taken.

3.4.1. Sample analysis

pH, Conductivity and Temperature

General samples were analysed directly after sampling for pH, conductivity, and temperature during the experiments. For this a WTW Multi 3630 IDS digital meter with a pH and conductivity sensor was used. The general samples were disposed of after analysis.

Total Organic Carbon

Total organic carbon (TOC) analysis was done at IHE Delft as the TOC analyser at the Waterlab was defective. Samples for TOC analysis were prepared according to the laboratory standard operating procedure (SOP TOC analyser). Samples were acidified with hydrochloric acid prior to analysis. Prepared samples were refrigerated until analysis.

PFAS

All sampling, sample preparation, instrumental analysis, and calibration-curve preparation were carried out according to the standard operating procedure (SOP preparation for Sciex). PFAS analysis was done using the Sciex 7500+ system at the Waterlab. Samples for PFAS analysis were prepared according to the laboratory SOP preparing and running PFAS samples for analysis on Sciex 7500+. For each sample, 500 µL of sample was mixed with 400 µL of Chromasolv ultrapure methanol and 100 µL of an internal standard solution (1 ng/mL). The mixture was vortexed and subsequently filtered through a 0.2 µm syringe filter (Chromafil Xtra 0.2 µm diameter 25 mm) into an LC-MS vial.

PFAS concentrations were determined by liquid chromatography–mass spectrometry (LC-MS). PFAS quantification was performed using internal standards added to each sample and corrected by calibration curves obtained through standards that were added to the analysis. Blanks and quality control samples were included as part of the quality assurance. PFAS analyses were performed in two batches. All CT and BD30 samples, as well as the effluent and foamate samples from the V1141 experiment, were analysed in the first batch. The remaining samples, including the V1141 influent sample, were analysed in the second batch. Potential batch-to-batch variations were therefore considered during interpretation of the PFAS results.

3.4.2. Data Analysis and Processing

Data processing and analysis were performed using Python (version 3.12.4) with the NumPy, Pandas, Matplotlib and Seaborn libraries. Experimental data were processed to calculate the performance indicators of the foam fractionation process, including enrichment factors, removal efficiencies, and mass balance percentage. In addition, limits of quantification (LOQs) were determined based on blank measurements and applied during data evaluation.

Limits of quantification (LOQs) were calculated according to Equation equation (3.2).

$$LOQ\,[ng/L] = C_{Blank} + 10 * SD_{Blank} \tag{3.2}$$

Where C_{Blank} is the mean concentration measured in the blank samples and SD_{Blank} is the standard deviation of the blank measurements. In total, six blanks were considered for LOQ computation. Calculated LOQs and lower bound calibration values are summarised in table 3.5. A complete overview of the blank measurements, calibration limits and LOQ values is provided in table A.2.

Component	LOQ [ng/L]	Low Cal.[ng/L]	Component	LOQ [ng/L]	Low Cal.[ng/L]
PFBA	2153.470	20.0	**PFOS**	7.595	1.0
PFPeA	8938.800	20.0	**FBSA**	1.324	10.0
PFHxA	101.118	2.0	**FHxSA**	5.103	1.0
PFHpA	3.714	1.0	**MeFOSAA**	16.736	1.0
PFOA	18.372	2.0	**EtFOSAA**	21.841	1.0
PFNA	2.091	1.0	**NaDONA**	19.807	1.0
PFtrDA	2168.680	100.0			

Table 3.5: Calculated LOQs and lowest calibration concentrations for PFAS compounds with non-zero blank concentrations.

Due to capacity limitations the PFAS analysis with the LC-MS was done in two different batches. The distribution of the samples across the batches can be seen in table 3.6. Due to big differences in blank concentrations between the two batches, some compounds have such high LOQ values. This is especially noticeable for PFBA, PFPeA and PFtrDA.

Batch	Experiment	Sample IDs
Batch 1	CT	IN, EF, Fo
Batch 1	BD30	IN, EF, Fo
Batch 1	V1141	EF, Fo
Batch 2	V1141	IN
Batch 2	AQUA	IN, EF, Fo
Batch 2	RO400	IN, EF, Fo
Batch 2	AM363	IN, EF, Fo
Batch 2	V1200	IN, EF, Fo

Table 3.6: Overview of experiments and samples included in analytical batch 1 and batch 2.

Equation (3.3) can be used to define the enrichment factor E where, C_{foam} is the concentration in the foamate and C_{in} the concentration in the influent. The removal efficiency (RE) can be defined using equation (3.4) where, C_{ef} is the concentration in the effluent.

$$E\,[-] = \frac{C_{foam}}{C_{in}} \tag{3.3}$$

$$RE\,[\%] = \left(1 - \frac{C_{ef}}{C_{in}}\right) * 100\% \tag{3.4}$$

To assess the overall recovery of PFAS throughout the experiments, a mass balance percentage was calculated according to equation (3.5). In this equation, Q represents the volumetric flow rate and C the PFAS concentration in the corresponding stream. Another method used to evaluate mass balance closure is the mass balance error as shown in equation (3.6). A mass balance close to 100% or an error close to zero indicates closure of the PFAS mass balance and provides confidence in the experimental results.

$$MB\,[\%] = \frac{Q_{ef} * C_{ef} + Q_{foam} * C_{foam}}{Q_{in} * C_{in}} * 100\% \tag{3.5}$$

$$Error\,[\%] = 100 - MB \tag{3.6}$$

Removal efficiencies, enrichment factors, and mass balances were calculated for individual PFAS compounds, PFAS grouped by functional group and chain length, as described in section 2.1.1 and table A.1, and the total PFAS concentration. Graphs and visualisations were generated using Matplotlib and Seaborn to support the interpretation and comparison of experimental results.

3.4.3. Additional Testing

Surface Tension Measurements

Surface tension measurements were conducted using the Du Noüy ring method. This method determines the force required to detach a platinum ring from the liquid surface, which is directly related to the surface tension of the solution. "Foam fractionation relies on the adsorption of surface-active compounds at the air-water interface. As the hypothesis of this thesis was that antiscalants might enhance PFAS adsorption to this interface by lowering the surface tension, surface tension measurements were performed to evaluate whether antiscalants influenced the surface activity of the different antiscalant solutions.

Viscosity Measurements

The dynamic viscosity of the solutions was determined using a Paar Physica UDS 200 rheometer. Measurements were performed to assess whether the presence of antiscalants affected the bulk fluid properties, which could influence bubble formation and foam behaviour during foam fractionation. All samples were measured under identical conditions and the recorded viscosity values were used for comparison between the different antiscalant solutions.

4

Results and Discussion

4.1. Influent Characteristics

4.1.1. Reverse Osmosis Concentrate

Analyses of the general chemical composition and PFAS concentrations of the RO concentrate were carried out by Het Waterlaboratorium (HWL) around the time the concentrate was collected. The measured chemical composition is shown in table 4.1.

Parameter	Value	Unit
DOC	15	mg/L as C
pH	8.23	-
Conductivity	2240	µS/cm
Turbidity	< 0.03	FTU
Barium	238	µg/L
Bicarbonate	929	mg/L
Calcium	350	mg/L
Chloride	275	mg/L
Magnesium	50.8	mg/L
Silicate	21.6	mg/L as SiO_2
Sodium	149	mg/L
Sulfate	245	mg/L as SO_4
ΣPFAS	86	ng/L

Table 4.1: Water quality parameters of RO concentrate measured at Het Waterlaboratorium.

The RO concentrate had a pH of 8.23, which is slightly alkaline, and a dissolved organic carbon (DOC) concentration of 15 mg/L as C. The turbidity was below the detection limit of <0.03 FTU, which is expected as ultrafiltration is used as a pre-treatment step prior to the reverse osmosis system.

Table 4.1 shows the concentrations of the ions associated with the target scalants presented in table 3.1. Bicarbonate was the highest measured anion, with a concentration of 929 mg/L, followed by chloride (275 mg/L) and sulfate (245 mg/L). Among the measured cations, calcium was present at the highest concentration (350 mg/L), followed by sodium (149 mg/L), magnesium (50.8 mg/L) and barium (238µg/L). The measured conductivity was 2240 µS/cm.

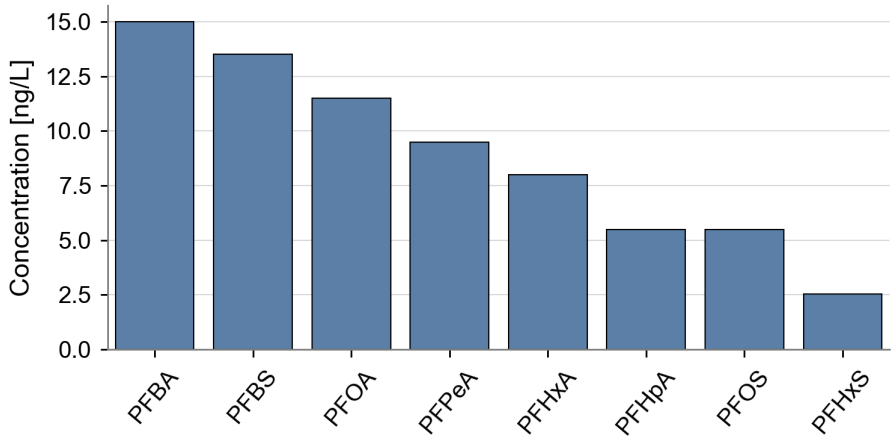

Figure 4.1: PFAS reporting by Dunea, converted to RO concentrate for a system with a removal efficiency of 80% [66].

Representative PFAS concentrations of the individual compounds in the RO concentrate are presented in figure 4.1 [66]. PFBA and PFBS were present at the highest concentrations, namely 15 ng/L and 13.5 ng/L, respectively. Both are considered short-chain PFAS. This was followed by PFOA and PFPeA, at 11.5 ng/L and 9.5 ng/L, respectively, while PFHxA and PFHpA were measured at 8 ng/L and 5.5 ng/L. PFOS and PFHxS showed the lowest concentrations, at 5.5 ng/L and 2.55 ng/L, respectively. Individual compounds with reported concentrations below the LOQ are not shown in the figure.

4.1.2. Field Blank

The field blank test was performed to verify that the column and experimental set-up were free from PFAS contamination and that adsorption to the column walls was negligible. Figure 4.2 shows the relative concentrations of PFAS exceeding the limit of quantification (LOQ). PFAS with concentrations below the LOQ were omitted from this visualisation.

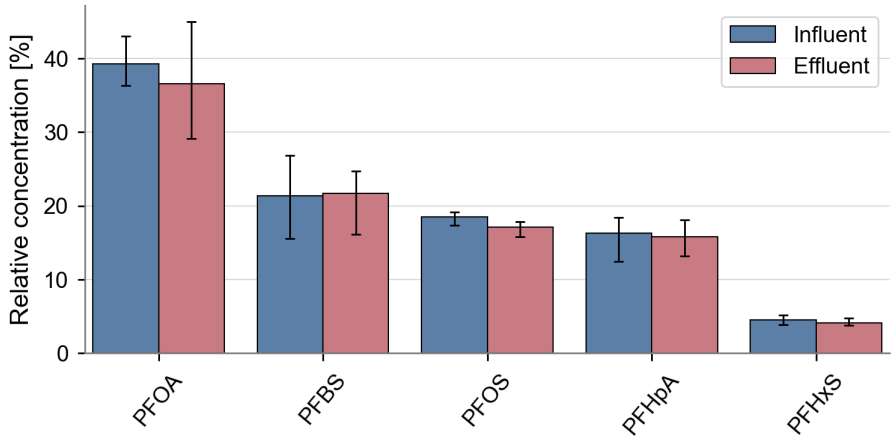

Figure 4.2: Mean relative concentrations of PFAS compounds measured in influent (n=3) and effluent (n=3) samples during the field blank test, expressed as a percentage of the total mean influent concentration. Error bars represent the relative minimum and maximum measured concentrations.

Table 4.2 presents the relative differences between influent and effluent concentrations. For all investigated PFAS compounds, these differences were below 10%, indicating that no significant contamination or adsorption occurred within the experimental set-up.

Compound	Difference [%]
PFOA	6.9
PFBS	1.5
PFOS	7.5
PFHpA	2.8
PFHxS	9.3

Table 4.2: Relative differences between mean influent and effluent concentrations for each PFAS detected in the field blank.

Figure 4.2 shows that PFOA represented a relatively large fraction of the total PFAS concentration in both the influent and effluent of the field blank. This corresponds to the relatively high PFOA concentration reported by HWL (figure 4.1). A similar trend was observed for PFOS and PFHpA, which also represented relatively large fractions of the total PFAS concentration in the field blank and were reported at relatively high concentrations by HWL. In contrast, PFBS and PFHxS represented smaller fractions of the total PFAS concentration in the field blank, consistent with their lower concentrations reported by HWL.

The mean ΣPFAS concentration in the influent of the field blank was lower than the ΣPFAS concentration in the RO concentrate measured by HWL. This difference can be explained by the fact that PFBA, PFPeA and PFHxA were not quantified in the field blank samples.

4.2. Bulk Liquid Properties

To evaluate whether antiscalant addition altered the physical properties of the RO concentrate, viscosity and surface tension measurements were performed for all antiscalants. The measured values are shown in table 4.3.

Experiment	Viscosity [mPa·s]	Surface Tension [mN/m]
CT	1.1	69.26
BD30	1.0	66.73
V1141	1.0	67.11
AM363	1.0	67.96
RO400	1.0	67.77
V1200	1.0	67.22
AQUA	1.0	67.72

Table 4.3: Measured viscosity and surface tension for all experiments.

The measured viscosities showed only minor differences between the untreated concentrate and the antiscalant-containing samples. The untreated concentrate exhibited a viscosity of approximately 1.1 mPa·s, whereas all samples containing antiscalants remained close to 1.0 mPa·s. Since viscosity can influence foam stability by affecting liquid drainage from foam films, a relevant change in viscosity could have affected foam structure or lifetime [50]. However, the almost identical values indicate that the antiscalants did not noticeably influence foam characteristics through changes in bulk viscosity. Kedir et al. [51] showed that adding SAV10 polymer below its critical overlap concentration ($c \approx 454$ ppm) improved foamability and foam stability, with only a small viscosity increase from about 1.2 to 1.8 mPa·s. In this study, the antiscalants were used at a much lower concentration (23.5 ppm). No significant viscosity increase was observed, which may be due

to the low concentration used.

The surface tension measurements showed that the untreated RO concentrate had a surface tension of approximately 70 mN/m. Following antiscalant addition, the surface tension decreased slightly and remained within a narrow range between approximately 67 and 68 mN/m. An additional control measurement with demineralised water resulted in a surface tension of 71.8 mN/m, which is slightly lower than the expected surface tension value for pure water of approximately 72 mN/m at 20 °C. Whereas common surfactants such as CTAB and SDS reduce surface tension to approximately 35 mN/m, the investigated antiscalants resulted in only a slight reduction, indicating that they had a negligible effect on the surface tension of the RO concentrate [67].

The limited reduction in surface tension is consistent with the chemical nature of most antiscalants. Antiscalants used in RO systems are generally not conventional surfactants, but are often anionic polymers or phosphorus-containing compounds with carboxylate, phosphonate or sulphonate functional groups [43][46]. These groups can interact with scale-forming ions and crystal surfaces but do not necessarily exhibit strong surface activity comparable to PFAS or co-surfactants. Therefore, at the relatively low concentrations applied in this study, the antiscalants may have slightly reduced surface tension without strongly affecting foam formation.

These findings were further supported by visual observations made during experiments to evaluate foam formation and foam stability.

Figure 4.3: Foam layer during experiments.

A representative photograph of the foam layer is shown in figure 4.3. In all experiments, only limited foam accumulation was observed. The foam layer was approximately 1–2 cm thick and collapsed almost immediately after the airflow was stopped, indicating that the foam was relatively unstable under the applied operating conditions. No clear effect of the antiscalants on foam characteristics was observed. No systematic differences in bubble size, foam height or overall foam structure were observed, suggesting that, under the applied conditions, the antiscalants did not strongly alter the macroscopic foam properties.

Overall, the results suggest that antiscalants slightly lowered the surface tension of the RO concentrate while having a negligible effect on viscosity. These limited changes in bulk liquid properties did not result in a clearly observable change in foam formation or foam characteristics. Therefore, any effect of antiscalants

on PFAS removal is expected to be mainly related to subtle matrix effects rather than to a strong change in bulk foam properties.

4.3. pH, Conductivity and TOC

The average pH and conductivity values measured in the influent, effluent and foamate during the experiments are presented in table 4.4. For each experiment, TOC analysis was performed for one influent sample and three effluent samples. These results can be found in table B.1. For all experiments, the pH of the effluent was higher than that of the influent, with increases ranging from 0.17 to 0.41 pH units.

Due to bubble injection, gas transfer occurred. The pH increased from approximately 8.0 to 8.3 after aeration. This increase is consistent with CO_2 stripping, whereby dissolved CO_2 is removed from the water, shifting the carbonate equilibrium towards CO_2 formation and consuming H^+ ions, resulting in a higher pH. Since the initial pH was already around 8, only a modest increase would be expected because the concentration of dissolved CO_2 decreases with increasing pH and the buffering capacity of the carbonate system limits further pH changes [68]. However, as alkalinity and dissolved inorganic carbon were not measured, this mechanism cannot be confirmed directly and other matrix-related effects cannot be excluded.

Conductivity values showed the opposite trend. Both effluent and foamate conductivities were generally lower than the influent conductivity. The observed decrease was relatively small, typically on the order of several percent. However, influent conductivity differed substantially between experiments, ranging from 1394 to 1954 µS/cm. The same pattern was observed in the effluent and foamate. Possible explanations for the conductivity differences between experiments include variability in the heterogeneity of the RO concentrate, differences in sample storage time or CO_2 exchange, and interactions between dissolved ions. Since individual ion concentrations were not measured during each experiment, the exact cause of the conductivity differences could not be identified.

	Average pH [-]			**Average Conductivity [µS/cm]**		
Experiment ID	*influent*	*effluent*	*foamate*	*influent*	*effluent*	*foamate*
CT	8.05	8.22	8.01	1935	1847	1840
BD30	8.00	8.34	8.34	1579	1577	1578
V1141	8.19	8.38	8.38	1394	1361	1380
AQUA	7.99	8.34	8.34	1826	1786	1796
RO400	7.91	8.32	8.32	1954	1854	1859
AM363	8.00	8.35	8.33	1415	1390	1391
V1200	7.93	8.33	8.32	1508	1504	1478

Table 4.4: Average pH and conductivity measured during the experiments.

TOC measurements were performed for the influent and effluent streams. The results can be found in table B.1. For most experiments, TOC concentrations in the effluent were similar to those measured in the influent, indicating limited removal of bulk organic matter during foam fractionation. However, interpretation of the TOC data is complicated by the fact that three samples were damaged, due to long sample storage times prior to analysis, and several measurements exceeded the detection range.

4.4. Overall Foam Fractionation Performance

The operational conditions during the foam fractionation experiments are summarised in table 4.5. The average influent flow rate (Q_{in}) varied between 80.7 mL/min and 83 mL/min, which is in close agreement with

the target flow rate of 82 mL/min. Similarly, the mean foamate fraction remained close to the target value of 20%, ranging from 15.9% to 21.6%. Although foamate fraction influences the balance between recovery and enrichment, the literature identifies other operating parameters, such as gas flow rate, bubble size and residence time, as more dominant factors for foam fractionation performance than the measured differences in foamate fraction [53][69][70]. Smith et al. [65] showed that decreasing the collected foam fraction primarily affects PFAS removal below approximately 10% foam recovery, whereas no statistically significant differences were observed between intermediate foam fractions. These findings suggest that the small differences in foamate fraction observed in the present study are unlikely to have substantially influenced the overall FF performance and that consistent operating conditions were maintained throughout the experiments in this research.

Experiment ID	Influent Flow	Foam%
CT	81.1	20.3%
BD30	80.7	19.0%
V1141	81.9	21.6%
AQUA	82.6	18.5%
RO400	83.0	21.3%
AM363	81.4	19.1%
V1200	82.5	15.9%

Table 4.5: Average influent flow and foam percentage for each experiment.

As shown in figure 4.4, the mean ΣPFAS removal efficiencies ranged from 64.8% to 79.2% between the investigated antiscalants. Error bars indicate the minimum and maximum mean ΣPFAS removal efficiencies observed for each antiscalant. The lowest mean ΣPFAS removal efficiency was observed for experiment V1141, while the highest mean ΣPFAS removal efficiency was achieved in the RO400 experiment. Compared with CT, which had a mean ΣPFAS removal efficiency of 71.8%, most experiments with antiscalants had a slightly higher mean ΣPFAS removal efficiency. However, the differences between most antiscalants remained relatively small.

A review article by We et al. [71] shows mean ΣPFAS removal efficiencies for different water matrices. Despite differences in water matrices and operational conditions, the mean ΣPFAS removal efficiencies ranging between 64.8% and 79.2% found in this research fall within the performance range reported in that article [71]. These results also correspond well with the removal efficiencies reported by Smith [29], who observed removals ranging from 63% to 84%. However, the mean ΣPFAS removal efficiencies found in this research are lower than the approximately 90% removal efficiency reported by McCleaf et al. [17] during foam fractionation of nanofiltration concentrate containing an antiscalant.

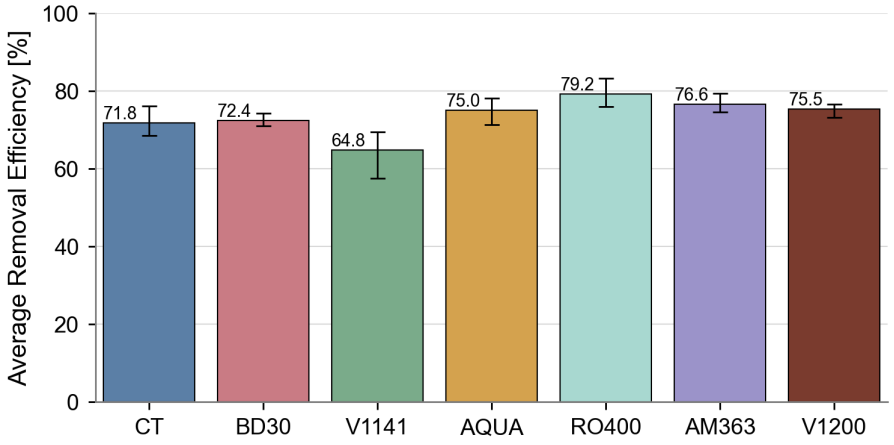

Figure 4.4: Removal efficiency per experiment.

Figure 4.5 shows the average ΣPFAS enrichment factors, with minimum and maximum enrichment indicated by the error bars. Considerable differences in enrichment were observed between the different experiments. The highest enrichment factor was observed for the BD30 experiment, which had an average enrichment factor of 6.86, followed by V1141 with an average enrichment factor of 6.43. The lowest enrichment factor was observed for AM363, at 2.48. These results correspond with enrichment factors reported in other lab-scale studies, where values varied between 2 and 30, with higher values usually corresponding to multi-stage foam fractionation [71].

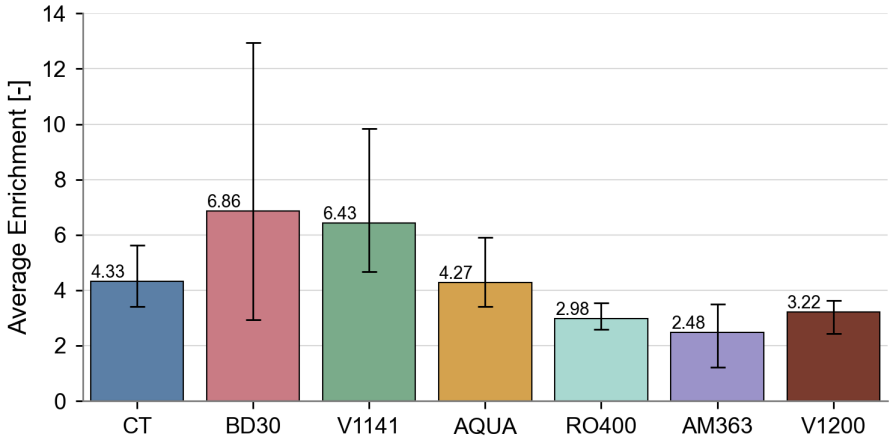

Figure 4.5: Enrichment factor per experiment.

Removal efficiency and enrichment factor provide complementary information. While removal efficiency mainly reflects the decrease in PFAS concentrations in the effluent, the enrichment factor provides information on the accumulation of PFAS in the foamate. However, enrichment factors should not be interpreted as stand-alone performance indicators, since the experiments with the highest enrichment factors also showed higher mass balance recoveries.

The recovery percentage of the mean ΣPFAS mass in the influent is shown in figure 4.6. For all experiments, most of the recovered ΣPFAS mass was detected in the foamate, whereas a smaller part of the ΣPFAS mass ended up in the effluent. The ΣPFAS mass percentage in the effluent was relatively stable, ranging from 16.3% to 27.6% of the measured influent PFAS mass, while foamate percentages ranged from 47.3% to 138.6% of the mean influent ΣPFAS mass. Smith et al. [72] reported similar results, where effluent concentrations were relatively constant but foam concentrations caused variability in mass balance closure.

Considerable differences in mass balance closure were observed between the different experiments. AQUA had the best mass balance closure, with a mean mass balance percentage of 99.4%, indicating near-complete recovery of the influent ΣPFAS mass. In contrast, BD30 and V1141 showed average recoveries above 100%, with recoveries ranging from 76.5% to 269.6% and from 124.6% to 245.6%, respectively. Overall, mean mass balance percentages ranged from 66% to 166%, indicating considerable differences in mass balance closure between experiments.

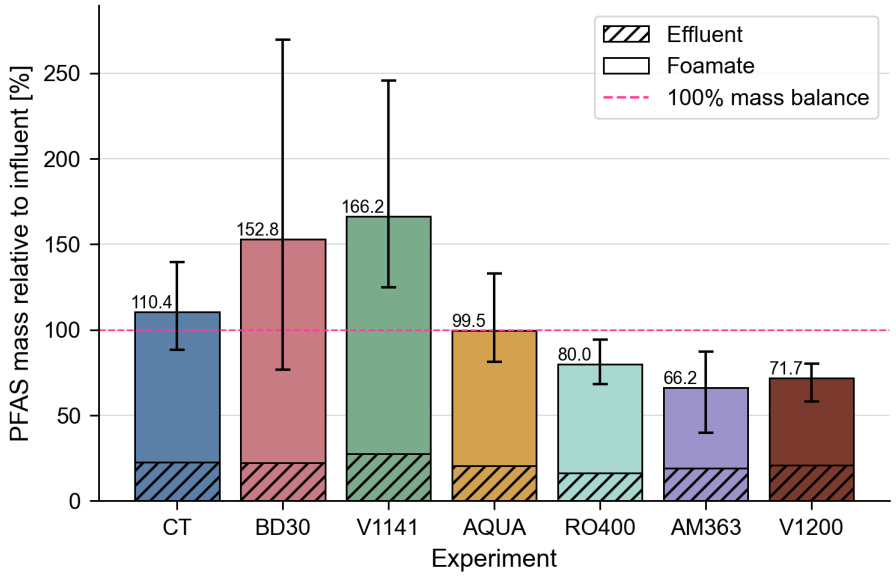

Figure 4.6: Total mass balance percentages per experiment.

4.5. Compound-Specific Behaviour

The influent, effluent and foamate concentrations for each compound are provided in section B.2.1. Figure 4.7 shows that the greatest variation in ΣPFAS concentrations between the experiments was found in the foamate. It also shows that, for all experiments, long-chain PFCAs and PFSAs were removed more effectively than short-chain PFCAs and PFSAs and the group of other PFAS. This is consistent with the literature. Sabba et al. [69] reported baseline removals of 10%–40% for short-chain PFAS in the absence of added co-surfactants or other enhancing agents, while long-chain PFAS were removed by 97%–99%. Similar trends have also been reported in other studies, where short-chain PFAS generally showed lower and more variable removal efficiencies than long-chain PFAS, which were removed more effectively, often exceeding 90% removal [17][73][65]. This can be explained by the higher hydrophobicity and surface activity of long-chain PFAS, which promotes adsorption at the air-water interface and transfer to the foam phase.

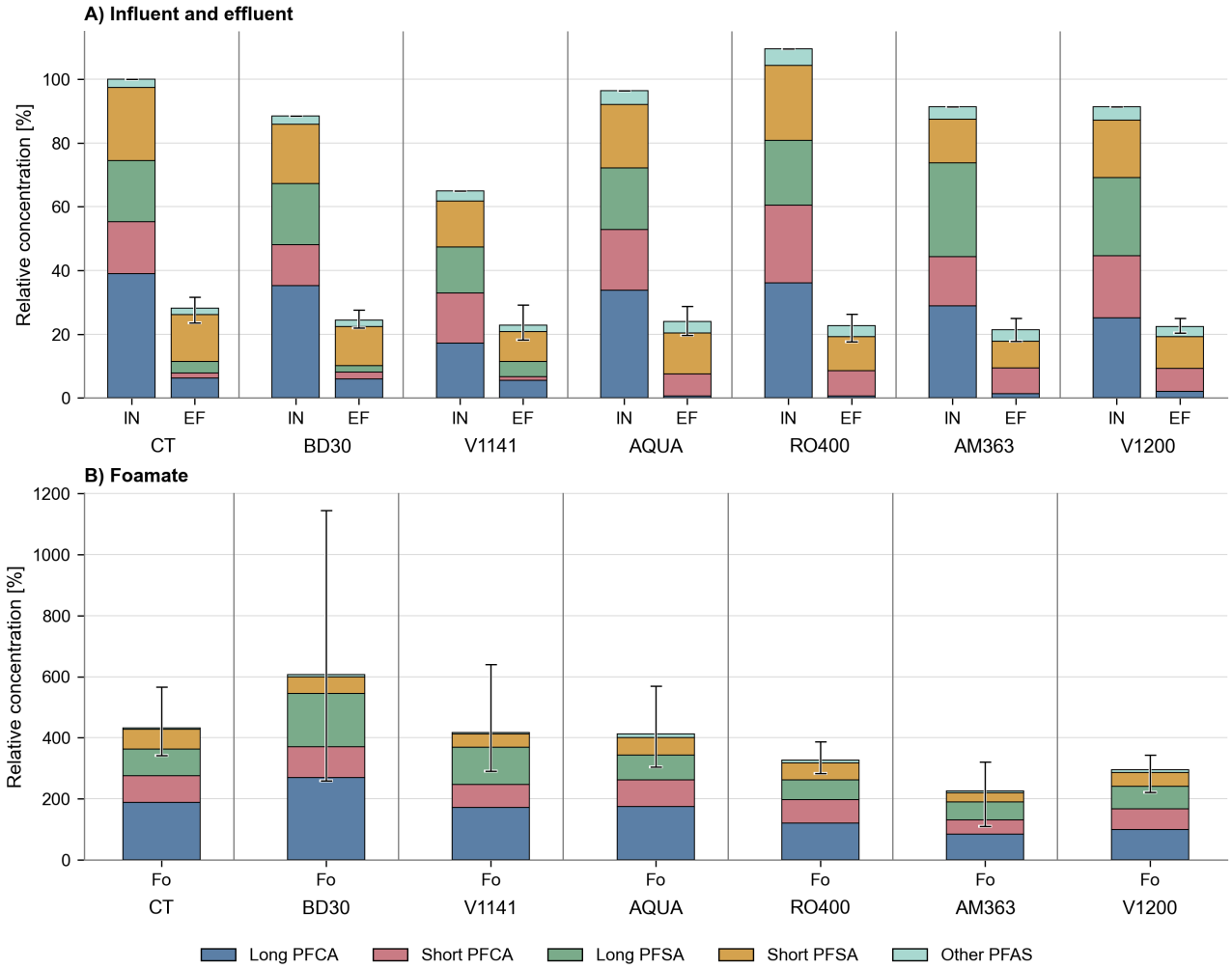

Figure 4.7: Summed PFAS concentrations relative to the total influent concentration of CT (set to 100%) grouped by compound class in the influent and effluent (A) and foamate (B) for each experiment. Bars represent mean relative concentrations, and error bars indicate the relative minimum and maximum measured values.

4.5.1. Compound-Specific Removal Efficiencies

Compound-specific removal efficiencies for all experiments are presented in figure 4.8, and a more detailed figure containing error values can be found in figure B.3.

Noticeable differences were observed between the individual PFAS compounds. The chain-length differences shown in figure 4.7 are confirmed by this figure. Among the investigated compounds, PFOA, PFHxS and PFOS, all longer-chain PFAS, exhibited the highest mean removal efficiencies, frequently approaching 100% across multiple experiments. It is important to note that apparent removal efficiencies of 100% do not necessarily indicate complete PFAS removal. Removal efficiencies of 100% should therefore be regarded as apparent removal efficiencies resulting from effluent concentrations that could not be reliably quantified, rather than as confirmed complete removal.

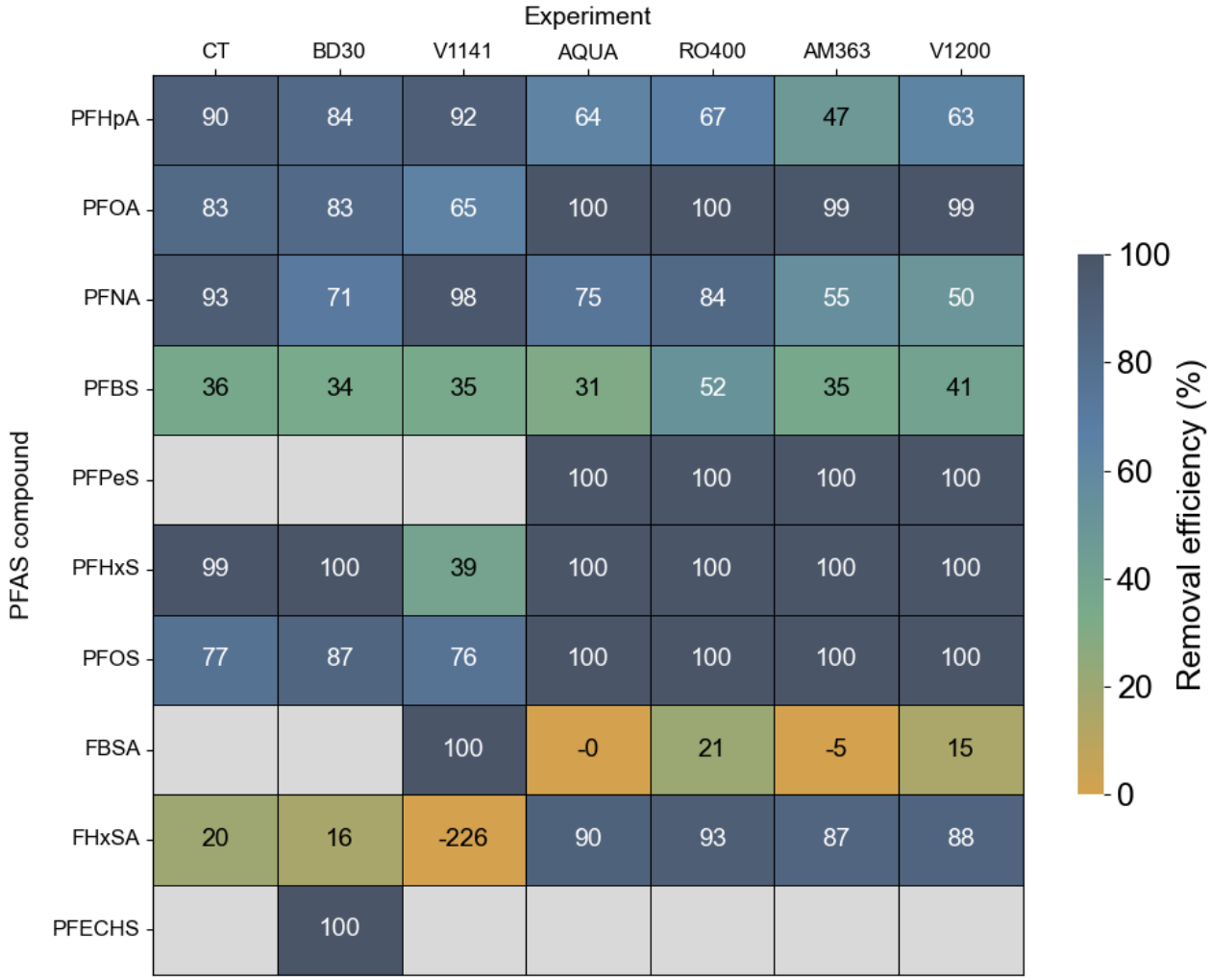

Figure 4.8: Compound-specific removal efficiencies.

PFBS, one of the short-chain PFAS, showed lower removal efficiencies, ranging from 31% to 52%. For PFBS, McCleaf et al. [17] found a removal efficiency of 34%, and Klevan et al. [74] found minimal to no removal of PFBS without the addition of a co-foaming agent. This may indicate that short-chain PFAS are more sensitive to matrix composition or operational conditions, since their partitioning to the air-water interface is weaker.

Overall, the removal patterns were relatively consistent across the investigated antiscalants. Nevertheless, some compound-specific irregularities were observed. For example, PFNA removal efficiencies varied considerably between experiments, ranging from 50% to 98%, while PFHpA removal ranged from 47% to 92%. Several compounds showed highly variable removal efficiencies across the experiments. For FBSA and FHxSA, this variability is likely related to differences between batches, as shown in table 3.6. FHxSA also showed substantial variation in removal efficiency across experiments, including a removal efficiency of -226% in the V1141 experiment, which can likely be attributed to batch differences as well.

4.5.2. Compound-Specific Enrichment and Mass Balance Closure

Compound-specific enrichment factors for all experiments are presented in figure 4.9, and a more detailed figure containing error values can be found in figure B.4.

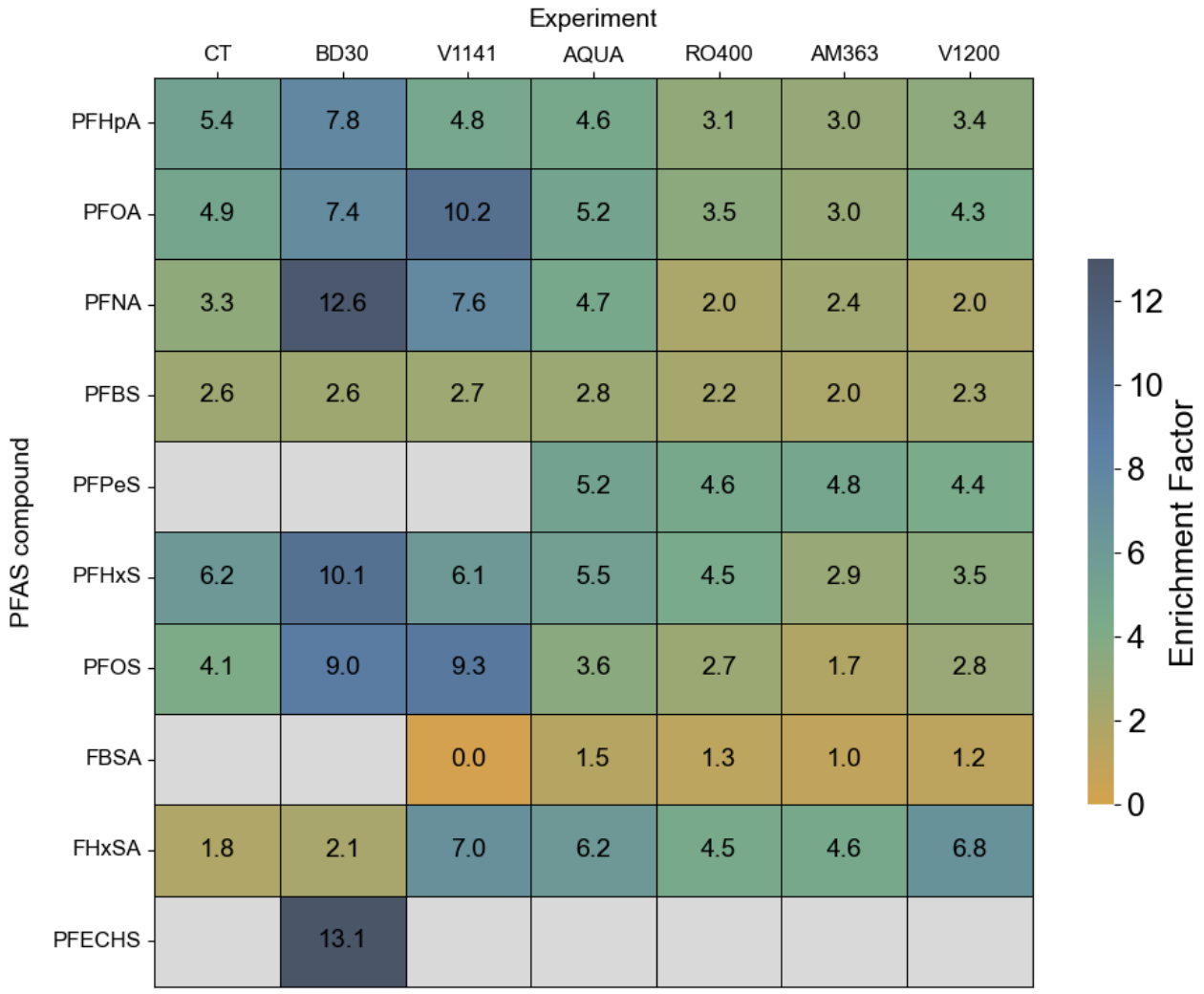

Figure 4.9: Compound-specific enrichment factors.

In contrast to the removal efficiencies, chain-length effects are less apparent in the enrichment factors. Nevertheless, PFBS consistently exhibited the lowest enrichment factors among the compounds for which enrichment could be calculated, with values ranging from 2.0 to 2.8 across all experiments. Relatively low enrichment factors were also observed for FBSA, although this compound could not be evaluated for the CT and BD30 experiments due to concentrations below the detection limit.

While enrichment patterns were generally similar across experiments, higher enrichment factors were observed for several compounds in the BD30 and V1141 experiments. This was particularly apparent for PFOA, PFNA and PFOS. In addition, the BD30 experiment showed elevated enrichment factors for PFHpA and PFHxS compared with the other experiments.

Figures 4.10 and 4.11 illustrate the mean PFOS and PFOA concentrations in the influent, effluent and foamate for all experiments. In figures 4.10a and 4.11a, all experiments are presented using a compound-specific LOQ, calculated using equation (3.2), to ensure a consistent comparison across the complete dataset. For PFOS, an LOQ of 7.59 ng/L was applied, whereas for PFOA an LOQ of 18.37 ng/L was used. Although the CT and BD30 samples were analysed in a separate analytical batch with lower LOQs of 2.54 ng/L for PFOS and 5.67 ng/L for PFOA, the higher LOQs from the first analytical batch were applied to all experiments to maintain comparability between experiments. As a result, several influent concentrations are shown

at or below the common LOQs. To illustrate the effect of the lower analytical background in the second analytical batch, figures 4.10b and 4.11b present the CT and BD30 experiments separately using their batch-specific LOQs. These figures show that the influent concentrations for CT and BD30 could be quantified with greater confidence under the lower LOQs, while the overall comparison throughout this research is based on a compound-specific LOQ.

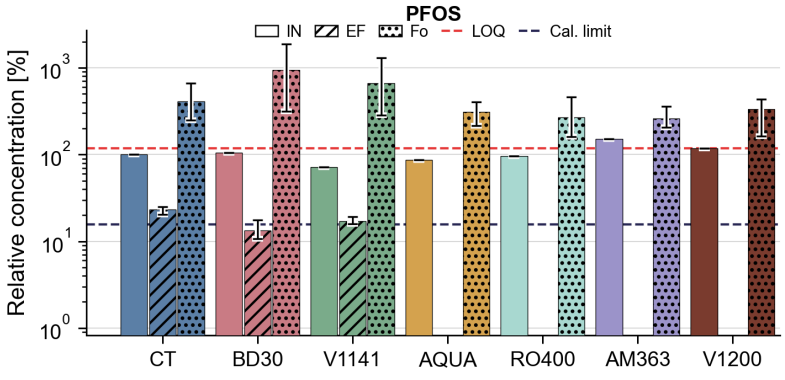

(a) All experiments using common LOQ.

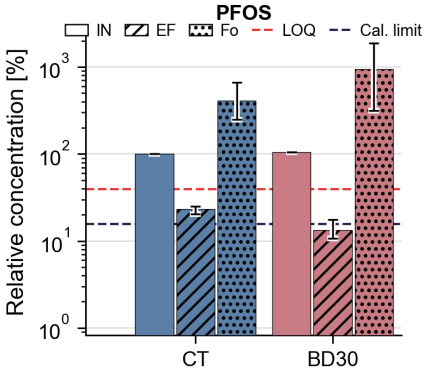

(b) CT and BD30 using batch-specific LOQ.

Figure 4.10: PFOS concentrations in the influent, effluent and foamate relative to the CT influent concentration (set to 100%). (a) shows all experiments on a common relative scale using the compound-specific LOQ, while (b) shows the CT and BD30 experiments using a lower, batch-specific LOQ. The dashed lines indicate the LOQ and calibration limit.

Overall, the influent and effluent concentrations remained relatively similar across the different antiscalants for PFOS and PFOA, although batch differences can be observed in the effluent. Substantially higher foamate concentrations were observed for the BD30 and V1141 experiments. This indicates that the higher enrichment factors and mass balance recoveries reported for these experiments were primarily driven by elevated PFAS concentrations in the foamate rather than by differences in influent or effluent concentrations.

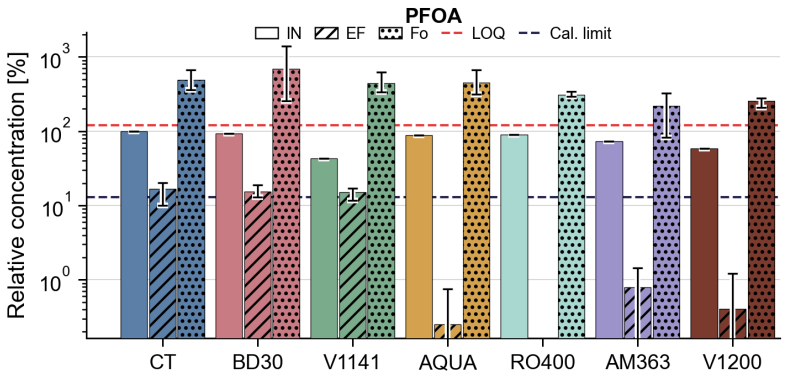

(a) All experiments using common LOQ.

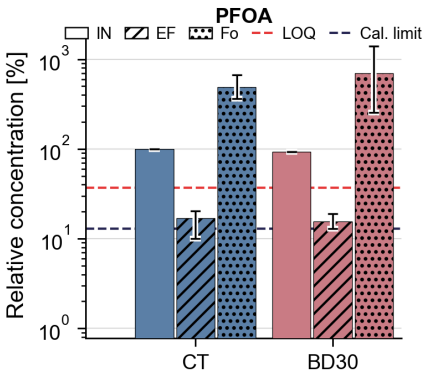

(b) CT and BD30 using batch-specific LOQ.

Figure 4.11: PFOA concentrations in the influent, effluent and foamate relative to the CT influent concentration (set to 100%). (a) shows all experiments on a common relative scale using the compound-specific LOQ, while (b) shows the CT and BD30 experiments using a lower, batch-specific LOQ. The dashed lines indicate the LOQ and calibration limit.

Since operational parameter variations were limited, as indicated in table 3.3, the observed differences in enrichment are more likely related to differences in the recovered PFAS mass than to variations in process operation. This relationship can be evaluated by examining the compound-specific mass balance recoveries presented in figure 4.12. Recovery percentages close to 100% indicate good mass balance closure, whereas values below or above 100% indicate under- or over-recovery, respectively. For most compounds and experiments, recoveries were within the approximate range of 80% to 120%, which is consistent with overall

recovery percentages ranging between 70% and 130% found by Wang et al. [55] and 120% ± 40% found by Smith et al. [75]. This indicates that the results of this thesis research are consistent with findings reported in the literature.

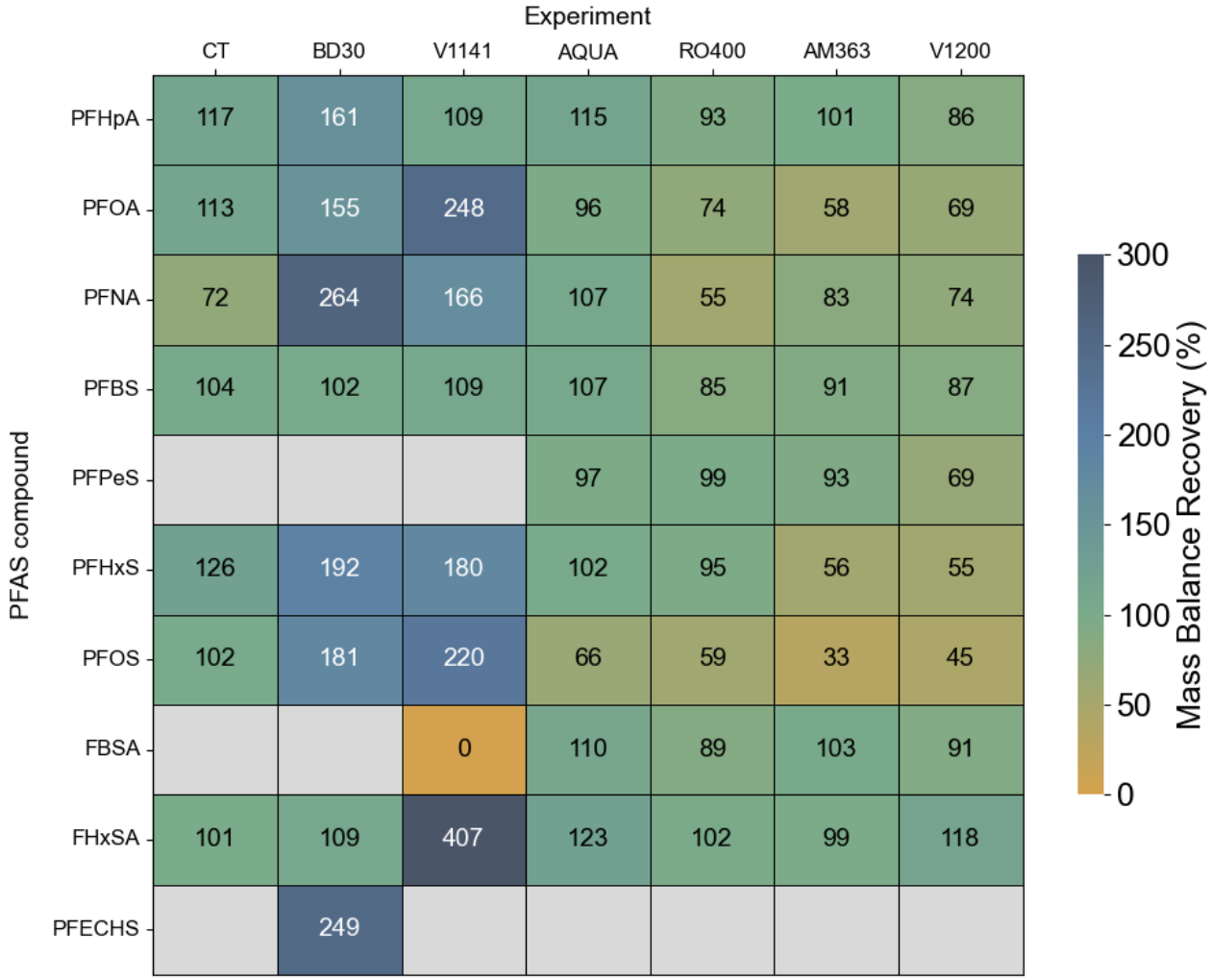

Figure 4.12: Compound-specific mass balance recovery.

Several notable values were observed. The BD30 and V1141 experiments showed multiple recoveries well above 100%, particularly for PFOA, PFNA, PFHxS and PFOS. The largest deviation was observed for FHxSA in the V1141 experiment, with a recovery of 407%, while all other experiments had reasonable recoveries for this compound. In contrast, lower recoveries were observed for some compounds in the AM363 and V1200 experiments, especially for PFOA, PFHxS and PFOS. As already shown in section 4.4, the mean ΣPFAS enrichment and mass balance percentages follow the same pattern. This is also apparent for individual compounds.

The similar pattern indicates that part of the variation in enrichment may be related to analytical variability in the foamate measurements. Therefore, the higher enrichment factors observed for BD30 and V1141 should be interpreted with caution and in combination with the corresponding mass balance closure.

Mass balance and enrichment variations were likely due to a combination of foam sampling variability, analytical uncertainty and the sensitivity of the mass balance calculation. As foamate samples were not taken from the bulk foamate but were sampled directly from the column, this introduced additional variability.

Since foam is dynamic, the collected sample may not fully represent the average foam produced during the experiment. PFAS concentrations in the foam are influenced by foam wetness, which is affected by gas flow rate, bubble size and foamate flow rate [71][70]. Slight variations in these parameters during sample collection can influence the PFAS concentrations in the foamate, causing variations in enrichment and mass balance.

This is particularly relevant in the present research, as many influent and effluent concentrations were below the LOQ or below the calibration minimum. These values were retained to avoid excluding a large part of the dataset. However, because they could not be reliably quantified, the corresponding removal efficiencies, enrichment factors and mass balance recoveries should be interpreted with caution.

As discussed by Smith et al. [75], the observed variation in mass balance might partly be explained by PFAS precursor compounds that were not included in the target analytical method. Targeted LC-MS does not capture all precursor compounds or unknown PFAS Balasuriya et al. [76]. Although Houtz et al. [77] showed that precursors can be converted to measurable PFAS under strong oxidative conditions, these conditions differ substantially from the aeration applied in the present study. Therefore, analytical uncertainty is considered a more likely explanation for the observed mass balance variation than precursor transformation.

4.6. Potential Influence of Antiscalants on PFAS Foam Fractionation

The investigated antiscalants did not produce large differences in the measured bulk liquid properties of the RO concentrate. However, differences in compound-specific enrichment and foamate concentrations were observed between the antiscalants, suggesting that their influence, if present, may have occurred through more subtle matrix-related interactions rather than through changes in bulk foam properties. An additional observation was the positive relationship between foam conductivity and the mean PFBS concentration in the foamate (Pearson's r=0.85, n=7; figure B.6). No comparable relationship was observed for the overall enrichment factor. As PFBS is one of the least hydrophobic and least surface-active PFAS investigated, this may suggest that short-chain PFAS are more sensitive to subtle variations in water chemistry than longer-chain PFAS. However, because conductivity was not varied as an independent experimental variable and only seven experimental conditions were available, this relationship should be regarded as exploratory rather than conclusive.

Although this observation cannot be interpreted as evidence for a specific mechanism, it is consistent with previous studies showing that changes in water chemistry can influence PFAS behaviour during foam fractionation. Zhou et al. [56] and Wang et al. [55] showed that changes in electrolyte composition can affect PFAS adsorption at the air-water interface by reducing electrostatic repulsion between surfactant head groups and increasing surface excess concentrations. Similarly, Wang et al. [78] demonstrated that multivalent cations can influence PFAS partitioning through cation bridging. While these studies do not directly explain the observations in the present work, they demonstrate that relatively subtle changes in matrix composition can affect PFAS behaviour.

This interpretation is also consistent with the original hypothesis of the present study. As discussed in the introduction, weakly interacting polymer–surfactant systems may modify foamability and interfacial behaviour without substantially changing the bulk physicochemical properties of the solution Petkova et al. [20]. In the present study, only minor changes in viscosity, surface tension and visible foam characteristics were observed following antiscalant addition, suggesting that any influence of the investigated antiscalants was not expressed through measurable changes in bulk foam properties. Instead, the compound-specific differences observed between experiments may be related to more subtle interactions between antiscalants, PFAS and the surrounding water matrix. However, these interactions were not investigated directly and therefore remain speculative.

5

Conclusion and Recommendations

5.1. Conclusion

This research investigated how different antiscalants influenced the performance and possible mechanisms of foam fractionation for the removal of PFAS from reverse osmosis concentrate originating from drinking water treatment. Overall, foam fractionation was able to remove a substantial fraction of the measured PFAS from the RO concentrate, while the influence of antiscalant type on the overall removal performance was limited under the applied experimental conditions.

The investigated antiscalants had only a minor effect on the bulk liquid properties and foam characteristics of the RO concentrate. Viscosity remained almost unchanged after antiscalant addition, while surface tension decreased only slightly compared with the control experiment. Visual observations also showed no clear differences in foam height, bubble structure, or foam stability between the experiments. In all cases, foam formation was limited and the foam collapsed rapidly after the airflow was stopped. This indicates that the tested antiscalants did not substantially influence foam formation or foam characteristics.

Mean ΣPFAS removal efficiencies ranged from 64.8% to 79.2% across the experiments. The control experiment showed a mean ΣPFAS removal efficiency of 71.8%, while the antiscalant-containing experiments showed comparable or only slightly different removal efficiencies. This suggests that antiscalant type did not strongly determine the total PFAS removal efficiency. Instead, removal was mainly governed by compound-specific PFAS properties. Long-chain PFAS, such as PFOA, PFHxS and PFOS, were removed more effectively than short-chain PFAS such as PFBS, which is consistent with their higher surface activity and stronger tendency to adsorb at the air-water interface.

Enrichment factors showed greater variation between experiments than removal efficiencies. The highest average enrichment factors were observed for BD30 and V1141, whereas the lowest enrichment factor was found for AM363. However, these differences were strongly related to elevated PFAS concentrations in the foamate and to mass balance recoveries above 100%. Therefore, the enrichment results should be interpreted with caution. Variability in foam sampling, foam wetness, analytical uncertainty and concentrations close to or below the LOQ likely contributed to the observed variation in enrichment factors and mass balance closure. As a result, enrichment factors alone were not sufficient to evaluate foam fractionation performance and should be interpreted together with removal efficiency and mass balance recovery.

The limited influence of the tested antiscalants can be explained by their low applied concentration and their chemical function. The antiscalants used in this study are not conventional surfactants and did not show strong surface activity in the RO concentrate. Although they may interact with scale-forming ions, crystal surfaces, or possibly with PFAS, these interactions were not clearly reflected in the measured foam characteristics or overall PFAS removal efficiency. Subtle matrix-related effects, for example involving dissolved ions, conductivity, or antiscalant-PFAS interactions, cannot be excluded, but they were not strong enough to cause a systematic change in foam fractionation performance.

The main research question can therefore be answered by concluding that the tested antiscalants had only a limited influence on the performance and mechanisms of foam fractionation for PFAS removal from drinking water RO concentrate. The antiscalants did not substantially change foam formation, foam stability, or overall ΣPFAS removal efficiency. Foam fractionation performance was mainly controlled by the surface-active properties of the individual PFAS compounds, rather than by the type of antiscalant present. Under the applied conditions, the presence of antiscalants therefore did not appear to inhibit foam fractionation for PFAS removal, although their possible influence on foamate enrichment and short-chain PFAS behaviour requires further investigation.

5.2. Recommendations

First, the practical relevance of further research should be evaluated in relation to the PFAS concentration of the investigated water matrix. The RO concentrate used in this study contained a relatively low ΣPFAS concentration compared with many PFAS-contaminated water streams. If the PFAS concentration of this specific matrix is already below current drinking water quality requirements, further optimisation of foam fractionation for this application may be less urgent from a drinking water perspective, especially as this water is treated to be returned to the environment and is not used as drinking water. However, additional research may still be relevant for RO concentrate management, discharge considerations, and water matrices with higher PFAS concentrations or a more challenging composition. Therefore, future work should preferably focus on matrices where PFAS removal from concentrate streams is expected to provide a clear regulatory, environmental, or operational benefit.

A second important recommendation is to improve the analytical reliability of the PFAS measurements. Preferably, all PFAS samples should be analysed within the same batch. If this is not possible, sufficient duplicate samples, quality controls, and inter-batch comparison samples should be included. This would reduce uncertainty related to batch-to-batch variation in LC-MS analysis, which was particularly relevant for the interpretation of some experiments, such as V1141. In addition, experiments with water streams containing higher PFAS concentrations could improve analytical reliability, reduce the influence of values close to or below the LOQ, and allow more robust mass balance calculations.

More detailed water quality analyses are also recommended. Future studies should quantify major ions, DOC or TOC, organic matter fractions and, if possible, residual antiscalant concentrations. More reliable TOC or DOC data would help determine whether organic matter or polymeric antiscalant components contribute to foam stability or PFAS partitioning. Together, these measurements would provide a stronger basis for determining whether antiscalants directly influence PFAS foam fractionation, or whether the observed differences are mainly caused by broader water matrix variability.

To better understand the possible mechanisms behind antiscalant effects, future experiments should include tests with higher antiscalant concentrations. Although these concentrations may not represent real-world RO operation, they could amplify matrix effects and help determine whether antiscalants influence PFAS partitioning, foam stability, or interactions between PFAS and dissolved ions.

Further research should also include a control experiment containing a cationic surfactant. This would confirm whether the experimental set-up is able to detect improved PFAS removal when interfacial interactions are strengthened. In addition, operational parameters such as gas flow rate, contact time, foamate fraction, pH, ionic strength and water level should be varied systematically, as these parameters can significantly affect PFAS removal efficiency.

Overall, these recommendations would help to improve both the reliability and the practical relevance of future research. By combining improved analytical methods, more detailed water quality characterisation and experiments with more relevant or challenging PFAS-containing matrices, future studies could better determine whether antiscalants have a direct influence on PFAS foam fractionation or whether observed variations are mainly caused by analytical uncertainty and broader water matrix effects.

References

[1] *Goal 6 | Department of Economic and Social Affairs*. URL: https://sdgs.un.org/goals/goal6#targets_and_indicators (visited on 04/03/2026).

[2] Suman Das and Avner Ronen. "A review on removal and destruction of per- and polyfluoroalkyl substances (PFAS) by novel membranes". In: *Membranes* 12.7 (June 2022), p. 662. DOI: 10.3390/membranes12070662. URL: https://doi.org/10.3390/membranes12070662.

[3] Water Environment Federation. *PFAS in the water and wastewater Sectors: Fundamentals, management, and treatment*. Water Environment Federation (WEF), 2023. ISBN: 978-1-57278-414-7. URL: https://app.knovel.com/hotlink/pdf/id:kt013DBL2H/pfas-in-water-wastewater/introduction-pfas-pfas.

[4] Robert C Buck et al. "Perfluoroalkyl and polyfluoroalkyl substances in the environment: Terminology, classification, and origins". In: *Integrated Environmental Assessment and Management* 7.4 (July 2011), pp. 513–541. DOI: 10.1002/ieam.258. URL: https://doi.org/10.1002/ieam.258.

[5] Rijksinstituut voor Volksgezondheid en Milieu. *Risico's PFAS voor gezondheid en milieu*. URL: https://www.rivm.nl/pfas/risicos-pfas-voor-gezondheid-en-milieu.

[6] Francisca Pérez et al. "Accumulation of perfluoroalkyl substances in human tissues". In: *Environment International* 59 (July 2013), pp. 354–362. DOI: 10.1016/j.envint.2013.06.004. URL: https://doi.org/10.1016/j.envint.2013.06.004.

[7] W. Bil et al. *PFAS in bloed van de Nederlandse bevolking*. Tech. rep. Rijksinstituut voor Volksgezondheid en Milieu, 2025. DOI: 10.21945/RIVM-2025-0094. URL: www.rivm.nl.

[8] US EPA. *Our current understanding of the human health and environmental risks of PFAS | US EPA*. Apr. 2026. URL: https://www.epa.gov/pfas/our-current-understanding-human-health-and-environmental-risks-pfas.

[9] *Directive (EU) 2020/2184 of the European Parliament and of the Council of 16 December 2020 on the quality of water intended for human consumption (recast)*. Directive. Dec. 23, 2020. URL: https://eur-lex.europa.eu/eli/dir/2020/2184/oj.

[10] *Drinkwaterbesluit (BWBR0030111)*. Algemene Maatregel van Bestuur. Geldend vanaf 01-01-2024; met bijlagen (onder meer Bijlage A) voor drinkwaterkwaliteitseisen. Jan. 1, 2024. URL: https://wetten.overheid.nl/BWBR0030111/2024-01-01.

[11] RIVM. *PFAS in drinkwater*. URL: https://www.rivm.nl/pfas/drinkwater.

[12] Dunea. *Dunea jaarverslag 2024*. URL: https://view.publitas.com/cfreport/dunea-jaarverslag-2024/page/1.

[13] Dunea. *PFAS*. URL: https://www.dunea.nl/drinkwater/waterkwaliteit-en-samenstelling/pfas?q=pfas.

[14] Giovanni Souza Casella et al. "Recent developments in membrane treatment technologies for PFAS removal from surface and groundwater". In: *Journal of environmental chemical engineering* 14.1 (Dec. 2025), p. 120598. DOI: 10.1016/j.jece.2025.120598. URL: https://doi.org/10.1016/j.jece.2025.120598.

[15] Thomas Buckley et al. "Review of foam fractionation as a water treatment technology". In: *Separation Science and Technology* 57.6 (July 2021), pp. 929–958. DOI: 10.1080/01496395.2021.1946698. URL: https://doi.org/10.1080/01496395.2021.1946698.

[16] Erik Kissa. *Fluorinated Surfactants and Repellents, Second Edition*. CRC Press, Feb. 2001.

[17] Philip McCleaf, William Stefansson, and Lutz Ahrens. "Drinking water nanofiltration with concentrate foam fractionation—A novel approach for removal of per- and polyfluoroalkyl substances (PFAS)". In: *Water Research* 232 (2023), p. 119688. DOI: 10.1016/j.watres.2023.119688.

[18] Jane Kucera. *Reverse Osmosis (3rd Edition)*. John Wiley Sons, 2023. ISBN: 978-1-119-72474-2. URL: https://app-knovel-com.tudelft.idm.oclc.org/s.v?tLPfSmls.

[19] Alice Antony et al. "Scale formation and control in high pressure membrane water treatment systems: A review". In: *Journal of Membrane Science* 383.1 (2011), pp. 1–16. ISSN: 0376-7388. DOI: https://doi.org/10.1016/j.memsci.2011.08.054. URL: https://www.sciencedirect.com/science/article/pii/S0376738811006430.

[20] R. Petkova, S. Tcholakova, and N.D. Denkov. "Foaming and foam stability for mixed polymer-surfactant solutions: Effects of surfactant type and polymer charge". In: *Langmuir* 28.11 (2012), pp. 4996–5009. DOI: 10.1021/la3003096. URL: https://www.scopus.com/inward/record.uri?eid=2-s2.0-84858781648&doi=10.1021%2fla3003096&partnerID=40&md5=356bad16b4fee1fc8b1f586d793b355e.

[21] RIVM. *PFAS*. URL: https://www.rivm.nl/en/pfas.

[22] Schmidt National Law Group. *Most Common Types if PFAS*. Oct. 2026. URL: https://www.nationalinjuryadvocates.com/most-common-types-of-pfas/.

[23] RIVM. *PFAS in drinkwater*. URL: https://www.rivm.nl/pfas.

[24] Ian T. Cousins et al. "The high persistence of PFAS is sufficient for their management as a chemical class". In: *Environmental Science Processes Impacts* 22.12 (Jan. 2020), pp. 2307–2312. DOI: 10.1039/d0em00355g. URL: https://doi.org/10.1039/d0em00355g.

[25] Interstate Technology & Regulatory Council (ITRC). *PFAS Technical and Regulatory Guidance Document and Fact Sheets*. Interstate Technology & Regulatory Council. 2026. URL: https://pfas-1.itrcweb.org/.

[26] National Center for Biotechnology Information. *Polytetrafluoroethylene*. PubChem. 2026. URL: https://pubchem.ncbi.nlm.nih.gov/compound/Polytetrafluoroethylene (visited on 05/30/2026).

[27] Joost Dalmijn et al. "HFPO-DA and other PFAS in air Downwind of a fluoropolymer production plant in the Netherlands: Measurements and modeling". In: *Environmental Science Technology* 59.17 (Apr. 2025), pp. 8662–8672. DOI: 10.1021/acs.est.4c13943. URL: https://pmc.ncbi.nlm.nih.gov/articles/PMC12060278/.

[28] John W. Washington et al. "Decades-Scale degradation of commercial, Side-Chain, Fluorotelomer-Based polymers in soils and water". In: *Environmental Science Technology* 49.2 (Nov. 2014), pp. 915–923. DOI: 10.1021/es504347u. URL: https://doi.org/10.1021/es504347u.

[29] Sanne Smith. *Innovative treatment technologies for PFAS-contaminated water - Utilizing foam partitioning and exploring electrochemical oxidation*. Uppsala, se: Swedish University of Agricultural Sciences, Department of Aquatic Sciences Assessment, Jan. 2023. DOI: 10.54612/a.6p8i5lbs8l. URL: https://doi.org/10.54612/a.6p8i5lbs8l.

[30] Aditya Choudhary et al. "Structure, orientation, and dynamics of per- and polyfluoroalkyl substance (PFAS) surfactants at the air-water interface: Molecular-level insights". In: *Journal of Colloid and Interface Science* 679.Pt A (Oct. 2024), pp. 1207–1218. DOI: 10.1016/j.jcis.2024.10.041. URL: https://doi.org/10.1016/j.jcis.2024.10.041.

[31] J.C van Dijk. *Nanofiltration and reverse osmosis*. 2007. URL: https://ocw.tudelft.nl/wp-content/uploads/Content.pdf.

[32] Begüm Tanis. *Introduction to Reverse Osmosis*. 2025. URL: https://brightspace.tudelft.nl/d2l/le/content/681231/viewContent/3962241/View.

[33] Laurence W. McKeen. *Markets and applications for films, containers, and membranes*. Elsevier eBooks, Oct. 21, 2011, pp. 59–75. DOI: 10.1016/b978-1-4377-3469-0.10004-9. URL: https://doi.org/10.1016/b978-1-4377-3469-0.10004-9.

[34] Ashok Kumar Nadda et al. *2. Sustainable Wastewater Treatment Using Membrane Technology*. 2023.

[35] Caihong Liu et al. "Evaluating the efficiency of nanofiltration and reverse osmosis membrane processes for the removal of per- and polyfluoroalkyl substances from water: A critical review". In: *Separation and Purification Technology* 302 (Sept. 2022), p. 122161. DOI: 10.1016/j.seppur.2022.122161. URL: https://doi.org/10.1016/j.seppur.2022.122161.

[36] Biotage. *PFAS Naming Convention Table*. Biotage. 2024. URL: https://www.biotage.com/hubfs/Unsorted%202024-%20Apr/1.%20DOCS%20DUMP%20%28APRIL%202024%29/PFAS%20Naming%20Convention%20-%20A4.pdf.

[37] National Center for Biotechnology Information. *PubChem Compound Summary for CID 6422, Trifluoroacetic acid*. 2026. URL: https://pubchem.ncbi.nlm.nih.gov/compound/Trifluoroacetic-acid (visited on 04/04/2026).

[38] Begüm Tanis. *Biofouling*. 2025. URL: https://brightspace.tudelft.nl/d2l/le/content/681231/viewContent/3962309/View.

[39] M. Nasir Mangal et al. "Scaling". In: *Seawater Reverse Osmosis Desalination: Assesment and Pre-treatment of Fouling and Scaling*. IWA Publishing, 2021. Chap. 8, pp. 207–230. DOI: 10.2166/9781780409863_0207.

[40] Begüm Tanis. *Scaling*. 2025. URL: https://brightspace.tudelft.nl/d2l/le/content/681231/viewContent/3962302/View.

[41] LibreTexts. *Solubility Product Constant, Ksp*. n.d. URL: https://chem.libretexts.org/Bookshelves/General_Chemistry/Map%3A_General_Chemistry_(Petrucci_et_al.)/18%3A_Solubility_and_Complex-Ion_Equilibria/18.1%3A_Solubility_Product_Constant_Ksp (visited on 04/04/2026).

[42] E.G. Darton. "Membrane chemical research: centuries apart". In: *Desalination* 132.1-3 (Dec. 2000), pp. 121–131. DOI: 10.1016/s0011-9164(00)00141-7. URL: https://doi.org/10.1016/s0011-9164(00)00141-7.

[43] Başak Keskin et al. "Insights to antiscalants in membrane processes: Types, inhibition mechanism and influencing factors". In: *Journal of Water Process Engineering* 75 (2025). DOI: 10.1016/j.jwpe.2025.107978.

[44] Wei Yu et al. "Antiscalants in RO membrane scaling control". In: *Water Research* 183 (June 18, 2020), p. 115985. DOI: 10.1016/j.watres.2020.115985. URL: https://doi.org/10.1016/j.watres.2020.115985.

[45] Musa Mpelwa and Shan-Fa Tang. "State of the art of synthetic threshold scale inhibitors for mineral scaling in the petroleum industry: a review". In: *Petroleum Science* 16 (2019). DOI: 10.1007/s12182-019-0299-5. URL: https://doi.org/10.1007/s12182-019-0299-5.

[46] Mahmoud A. Ahmed and Ashraf A. Mohamed. "Evaluation and optimization of antiscalant substances for enhanced reverse osmosis performance". In: *Journal of Saudi Chemical Society* 28 (2024). DOI: 10.1016/j.jscs.2024.101923. URL: https://doi.org/10.1016/j.jscs.2024.101923.

[47] Dictionary.com. *Definition of amphiphilic*. URL: https://www.dictionary.com/browse/amphiphilic.

[48] Paul Stevenson and Xueliang Li. *Foam Fractionation*. CRC Press, 2014. ISBN: 9780429098000.

[49] Raziyeh Dehghani et al. "A comprehensive review on key mechanisms and parameters affecting foam stability". In: *Journal of Molecular Liquids* 416 (Nov. 14, 2024), p. 126477. DOI: 10.1016/j.molliq.2024.126477. URL: https://doi.org/10.1016/j.molliq.2024.126477.

[50] Zhoujie Wang et al. "Advances and challenges in foam stability: Applications, mechanisms, and future directions". In: *Capillarity* 15.3 (May 2025), pp. 58–73. DOI: 10.46690/capi.2025.06.02. URL: https://doi.org/10.46690/capi.2025.06.02.

[51] Abduljelil S. Kedir, Jonas S. Solbakken, and Morten G. Aarra. "Foamability and stability of anionic surfactant-anionic polymer solutions: Influence of ionic strength, polymer concentration, and molecular weight". In: *Colloids and Surfaces A Physicochemical and Engineering Aspects* 632 (Oct. 2021), p. 127801. DOI: 10.1016/j.colsurfa.2021.127801. URL: https://doi.org/10.1016/j.colsurfa.2021.127801.

[52] Wiebke Drenckhan and Arnaud Saint-Jalmes. "The science of foaming". In: *Advances in Colloid and Interface Science* 222 (Apr. 2015), pp. 228–259. DOI: 10.1016/j.cis.2015.04.001. URL: https://doi.org/10.1016/j.cis.2015.04.001.

[53] J. Merz et al. "Continuous foam fractionation: Performance as a function of operating variables". In: *Separation and Purification Technology* 82 (July 2011), pp. 10–18. DOI: 10.1016/j.seppur.2011.07.023. URL: https://doi.org/10.1016/j.seppur.2011.07.023.

[54] Robert Lemlich. "Adsorptive Bubble Separation Methods—Foam Fractionation and Allied Techniques". In: *Industrial & Engineering Chemistry* 60.10 (1968), pp. 16–29. DOI: 10.1021/ie50706a005. URL: https://doi.org/10.1021/ie50706a005.

[55] Yifei Wang et al. "Removing per- and polyfluoroalkyl substances (PFAS) in water by foam fractionation". In: *Chemosphere* 311.Pt 2 (Oct. 2022), p. 137004. DOI: 10.1016/j.chemosphere.2022.137004. URL: https://doi.org/10.1016/j.chemosphere.2022.137004.

[56] Muchu Zhou et al. "Influence of electrolytes on the Air–Water interfacial properties of perfluoroalkyl acids (PFAAs)". In: *Langmuir* 42.9 (Feb. 2026), pp. 6623–6636. DOI: 10.1021/acs.langmuir.5c04005. URL: https://doi.org/10.1021/acs.langmuir.5c04005.

[57] Wageningen University & Research. *eDepot Publication 339532*. 2015. URL: https://edepot.wur.nl/339532.

[58] Wasseraufbereitung Shop24. *Vitec 1141 Datasheet*. n.d. URL: https://www.wasseraufbereitung-shop24.de/media/files_public/915016798c590c7fa9570e76c99d9a36/Datenblatt-Vitec-1141.pdf.

[59] Wasseraufbereitung Shop24. *Vitec 1141 Antiscalant*. n.d. URL: https://www.wasseraufbereitung-shop24.de/de/zubehoer/chemikalien/antiscalant/vitec-1141.

[60] Aquatreat. *Reverse Osmosis*. n.d. URL: https://aquatreat.eu/r-o/.

[61] BASF. *Sokalan 400 Datasheet*. n.d. URL: https://5.imimg.com/data5/BX/LP/MY-3034436/sokalan-400.pdf.

[62] Reaxial. *Antiaskalants for Reverse Osmosis*. n.d. URL: https://reaxial.com/catalog/filtration-installations/reagents-for-ro/antiaskalants/id278.

[63] Lenntech. *Vitec 1200 Liquid Antiscalant*. n.d. URL: https://www.lenntech.nl/producten/Avista/Vitec-1200/Vitec-1200-liquid-AntiScalant/index.html.

[64] Philip McCleaf, Ylva Kjellgren, and Lutz Ahrens. "Foam fractionation removal of multiple per- and polyfluoroalkyl substances from landfill leachate". In: *AWWA Water Science* 3.5 (Sept. 2021). DOI: 10.1002/aws2.1238. URL: https://doi.org/10.1002/aws2.1238.

[65] Sanne J. Smith et al. “Pilot-Scale Continuous Foam Fractionation for the Removal of Per- and Polyfluoroalkyl Substances (PFAS) from Landfill Leachate”. In: *ACS EST Water* 2.5 (May 2022), pp. 841–851. DOI: 10.1021/acsestwater.2c00032. URL: https://doi.org/10.1021/acsestwater.2c00032.

[66] Dunea. *Meetgegevens PFAS*. 2026. URL: https://www.dunea.nl/drinkwater/waterkwaliteit-en-samenstelling/pfas/meetgegevens-pfas.

[67] Mohamed A. Bahri et al. “Investigation of SDS, DTAB and CTAB Micelle Microviscosities by Electron Spin Resonance”. In: *Colloids and Surfaces A: Physicochemical and Engineering Aspects* 290.1–3 (2006), pp. 206–212. DOI: 10.1016/j.colsurfa.2006.05.021. URL: https://doi.org/10.1016/j.colsurfa.2006.05.021.

[68] J.C van Dijk. *Aeration and gas stripping in water treatment*. 2007. URL: https://ocw.tudelft.nl/wp-content/uploads/Aeration-and-gas-stripping-1.pdf.

[69] Fabrizio Sabba et al. “Optimizing foam fractionation for PFAS removal from landfill leachate: treatment performance and operational insights”. In: *The Science of The Total Environment* 1010 (Jan. 2026), p. 181050. DOI: 10.1016/j.scitotenv.2025.181050. URL: https://doi.org/10.1016/j.scitotenv.2025.181050.

[70] Mateusz Sochacki, Piotr Michorczyk, and Otmar Vogt. “Foam fractionation as an efficient method for the separation and recovery of surfactants and Surface-Inactive agents: state of the art”. In: *ACS Omega* 10.1 (Dec. 2024), pp. 55–75. DOI: 10.1021/acsomega.4c08413. URL: https://doi.org/10.1021/acsomega.4c08413.

[71] Angel Chyi En We et al. “A review of foam fractionation for the removal of per- and polyfluoroalkyl substances (PFAS) from aqueous matrices”. In: *Journal of Hazardous Materials* 465 (Dec. 2023), p. 133182. DOI: 10.1016/j.jhazmat.2023.133182. URL: https://doi.org/10.1016/j.jhazmat.2023.133182.

[72] Sanne J. Smith et al. “Electrochemical Oxidation for treatment of PFAS in Contaminated water and fractionated Foam⊠A Pilot-Scale Study”. In: *ACS EST Water* 3.4 (Mar. 2023), pp. 1201–1211. DOI: 10.1021/acsestwater.2c00660. URL: https://doi.org/10.1021/acsestwater.2c00660.

[73] Phong H.N. Vo et al. “Foam fractionation of per- and polyfluoroalkyl substances (PFASs) in landfill leachate using different cosurfactants”. In: *Chemosphere* 310 (Oct. 2022), p. 136869. DOI: 10.1016/j.chemosphere.2022.136869. URL: https://doi.org/10.1016/j.chemosphere.2022.136869.

[74] Craig Klevan et al. “Removal of long- and short-chain PFAS from groundwater by foam fractionation”. In: *Environmental Science Water Research Technology* 11.10 (Jan. 2025), pp. 2295–2307. DOI: 10.1039/d5ew00440c. URL: https://doi.org/10.1039/d5ew00440c.

[75] Sanne J. Smith et al. “Foam fractionation for removal of per- and polyfluoroalkyl substances: Towards closing the mass balance”. In: *The Science of The Total Environment* 871 (Feb. 2023), p. 162050. DOI: 10.1016/j.scitotenv.2023.162050. URL: https://doi.org/10.1016/j.scitotenv.2023.162050.

[76] Damalka Balasuriya et al. “The hidden fluorine: a critical review of analytical methods for unmasking PFAS and closing fluorine mass balance in environmental samples”. In: *Analytical and Bioanalytical Chemistry* 418.12 (Apr. 2026), pp. 3489–3508. DOI: 10.1007/s00216-026-06458-6. URL: https://doi.org/10.1007/s00216-026-06458-6.

[77] Erika F. Houtz and David L. Sedlak. “Oxidative conversion as a means of detecting precursors to perfluoroalkyl acids in urban runoff”. In: *Environmental Science Technology* 46.17 (Aug. 2012), pp. 9342–9349. DOI: 10.1021/es302274g. URL: https://doi.org/10.1021/es302274g.

[78] Wenfeng Wang et al. “Implication of cation-bridging interaction contribution to sorption of perfluoroalkyl carboxylic acids by soils”. In: *Chemosphere* 290 (Dec. 2021), p. 133224. DOI: 10.1016/j.chemosphere.2021.133224. URL: https://doi.org/10.1016/j.chemosphere.2021.133224.

A

Analytical Information and PFAS Classification

A.1. PFAS Classification by Compound Group and Chain Length

Table A.1 provides the compound classification used for the PFAS results. The PFAS compounds were grouped according to their chemical class and chain length. This classification was used to distinguish between short-chain and long-chain PFAS and to support the discussion of differences in removal efficiency, enrichment and mass balance behaviour.

PFAS Group	PFAS
Long PFCAs	PFOA, PFNA, PFDA, PFUnDA, PFDoDA, PFtrDA, PFTeDA
Long PFSAs	PFHxS, PFHpS, PFOS, PFNS, PFDS
Short PFCAs	PFBA, PFPeA, PFHxA, PFHpA
Short PFSAs	PFBS, PFPeS
Other PFAS	4:2 FTSA, 6:2 FTSA, 8:2FTSA, HFPO-DA (GenX), NaDONA, MeFBSAA, FBSA, 9Cl-PF3ONS, FHxSA, PFECHS, EtFOSAA, MeFOSAA, 11Cl-PF3OUdS, FOSA

Table A.1: All analysed PFAS grouped

A.2. Limits of Quantification

The limits of quantification (LOQs) used for the PFAS analyses are presented in table A.2. These values were used to assess the reliability of the measured PFAS concentrations. Measurements below the LOQ were retained in the dataset to avoid excluding a large part of the results, but were interpreted with caution.

MeFBSAA, HFPO-DA, PFBS, PFPeS, PFHxS, PFHpS, PFECHS, FOSA, PFDA, PFDS, PFTeDA, 4:2 FTSA, 8:2 FTSA, 9Cl-PF3ONS and PFUnDA were not included in the figure as the blank average, blank standard deviation en LOQ were not quantified due to quantification limits.

Component	Low Cal.	LOQ Batch 1			LOQ Combined Batches		
		Blank Avg.	Blank Std.	LOQ	Blank Avg.	Blank Std.	LOQ
PFBA	20.0	0.000	0.000	0.000	179.246	197.422	2153.470
PFPeA	20.0	0.000	0.000	0.000	720.325	821.848	8938.800
PFHxA	2.0	24.497	2.167	46.166	17.079	8.404	101.118
PFHpA	1.0	0.645	0.232	2.966	0.378	0.334	3.714
PFOA	2.0	3.060	0.261	5.667	1.530	1.684	18.372
PFNA	1.0	0.254	0.220	2.449	0.127	0.196	2.091
PFOS	1.0	1.365	0.117	2.537	0.773	0.682	7.595
FBSA	10.0	0.000	0.000	0.000	0.052	0.127	1.324
FHxSA	1.0	0.891	0.075	1.646	0.475	0.463	5.103
PFDoDA	0.0	0.000	0.000	0.000	0.005	0.012	0.120
PFtrDA	100.0	362.807	3.156	394.364	181.404	198.728	2168.680
MeFOSAA	1.0	0.000	0.000	0.000	0.698	1.604	16.736
EtFOSAA	1.0	0.000	0.000	0.000	1.011	2.083	21.841
NaDONA	1.0	3.090	1.114	14.234	1.552	1.825	19.807
6:2 FTSA	0.0	0.000	0.000	0.000	0.442	0.636	6.803
11Cl-PF3OUdS	0.0	1.490	0.321	4.703	0.818	0.780	8.618

Table A.2: Blank averages, blank standard deviations and calculated LOQs for different PFAS

A.3. Calibration Curves and Calibration Ranges

The calibration curve information for the analysed PFAS compounds is presented in table A.3. These data were used to evaluate whether measured concentrations were within the reliable calibration range of the analytical method. Measurements below the calibration minimum were retained in the dataset to avoid excluding a large part of the results, but were interpreted with caution.

Component	Low Cal.	Component	Low Cal.
PFBA	20.0	**PFBS**	10.0
PFPeA	20.0	**PFPeS**	2.0
PFHxA	2.0	**PFHxS**	2.0
PFHpA	1.0	**PFHpS**	2.0
PFOA	2.0	**PFOS**	1.0
PFNA	1.0	**PFNS**	2.0
PFDA	1.0	**PFDS**	2.0
PFUnDA	1.0	**FBSA**	10.0
PFDoDA	0.0	**FHxSA**	1.0
PFtrDA	100.0	**FOSA**	10.0
PFTeDA	10.0	**MeFOSAA**	1.0
MeFBSAA	10.0	**EtFOSAA**	1.0
HFPO-DA	10.0	**4:2 FTSA**	0.2
NaDONA	1.0	**6:2 FTSA**	0.0
PFECHS	1.0	**8:2 FTSA**	1.0
9Cl-PF3ONS	2.0	**11Cl-PF3OUdS**	0.0

Table A.3: Minimum calibration concentrations for the analysed PFAS compounds.

B

Supplementary Compound Specific Results

B.1. Additional Water Quality Results

Table B.1 presents additional water quality results measured during the foam fractionation experiments.

	Influent	Results (TOC)		
Experiment	**IN**	**EF1**	**EF2**	**EF3**
CT	18.7	17.7	18.4	18.4
AQUA	>20	–	>20	19.4
RO400	>20	>20	>20	>20
V1200	–	>20	17.5	–
AM363	14.9	14.8	15.1	15.3
V1141	15.8	13.7	14.4	14.3
BD30	16.6	17.8	17.2	16.4

Table B.1: Reported TOC concentrations for influent and effluent samples of the different experiments

B.2. Compound-Specific PFAS Concentrations

This section presents the compound-specific PFAS concentrations measured in the influent, effluent and foamate samples for each experiment. These data provide the basis for the calculated removal efficiencies, enrichment factors and mass balance recoveries discussed in the main text. The results are included in the appendix because the full compound-specific dataset is too detailed to present in the main results chapter.

B.2.1. Individual PFAS Results

Figure B.1 and figure B.2 present the individual PFAS concentration profiles for the investigated compounds. The bars represent the mean measured concentrations, while the error bars indicate the minimum and maximum measured values.

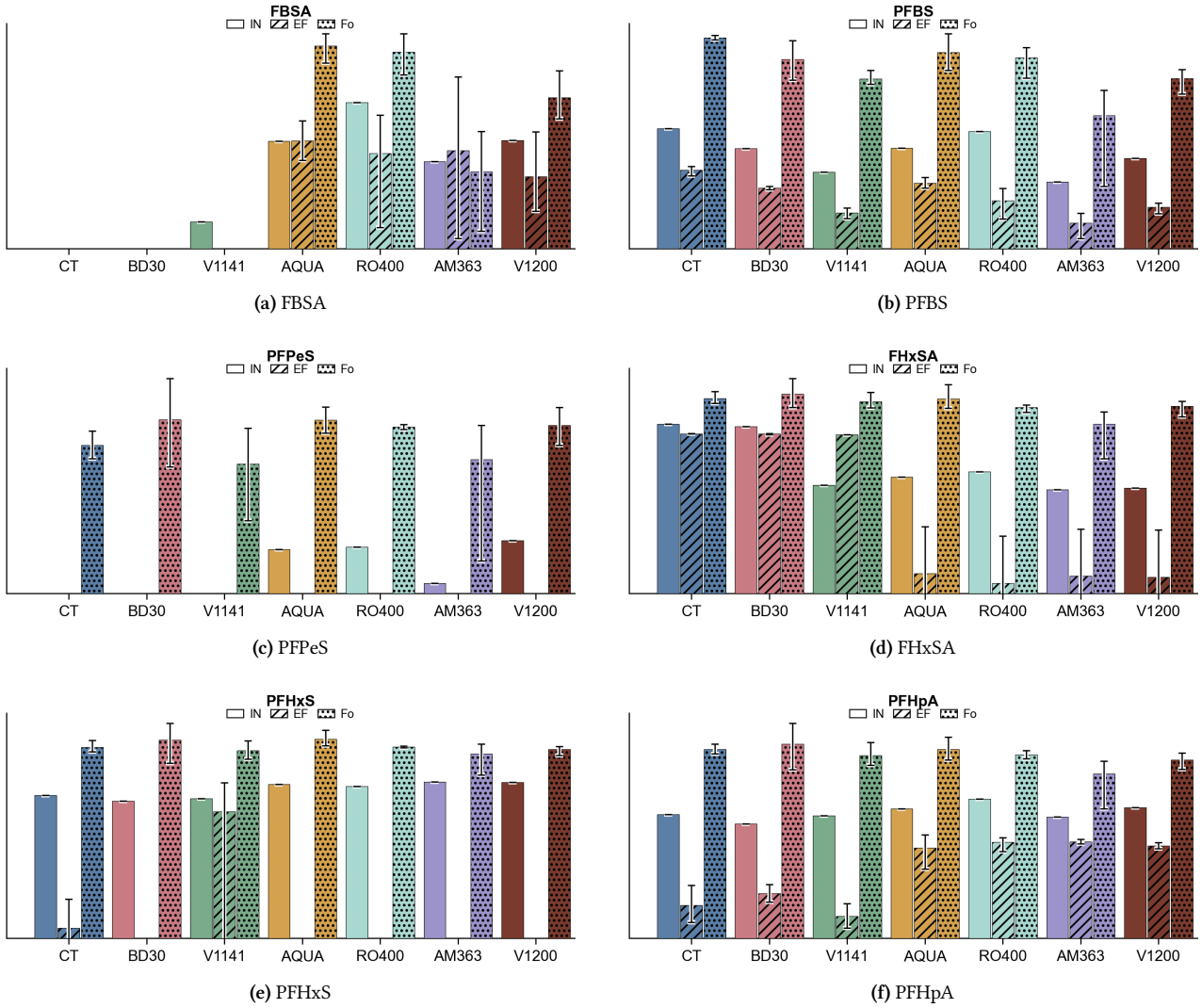

(a) FBSA **(b)** PFBS

(c) PFPeS **(d)** FHxSA

(e) PFHxS **(f)** PFHpA

Figure B.1: Compound-specific PFAS concentrations. The bars represent the mean measured concentrations, and the error bars indicate the minimum and maximum measured values.

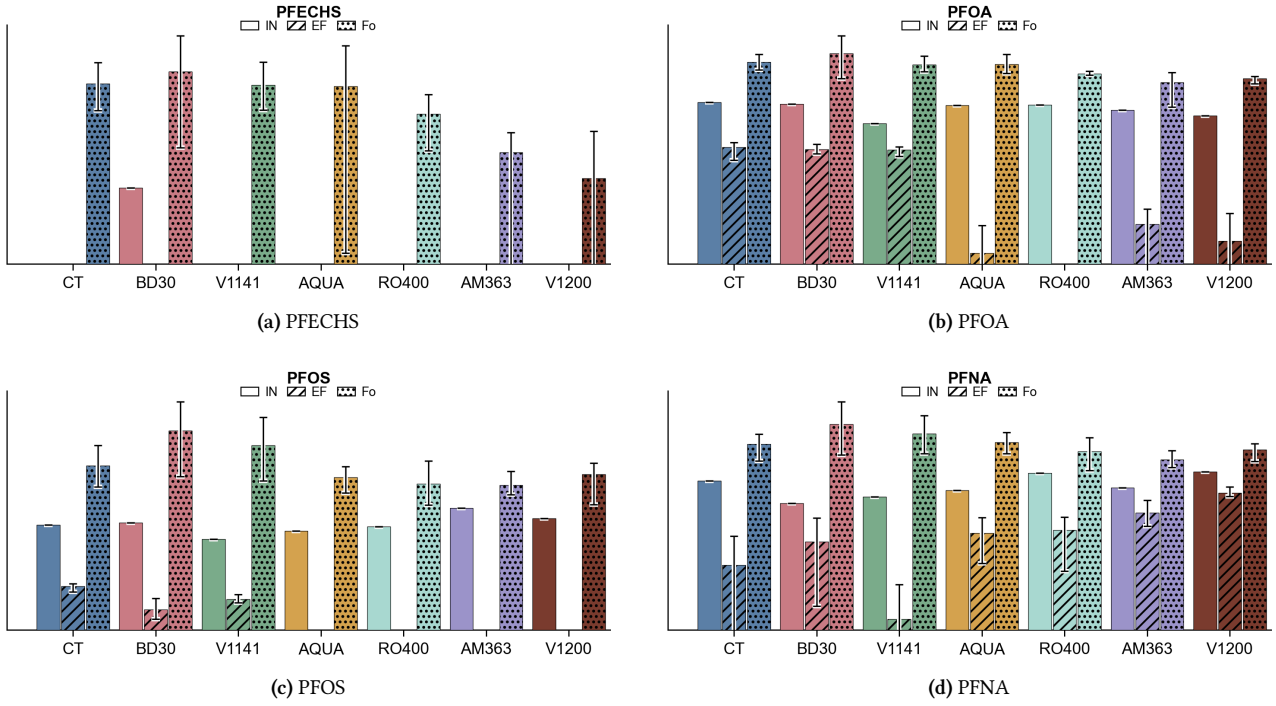

(a) PFECHS **(b)** PFOA

(c) PFOS **(d)** PFNA

Figure B.2: Compound-specific PFAS concentrations. The bars represent the mean measured concentrations, and the error bars indicate the minimum and maximum measured values.

B.2.2. Compound-Specific Removal Efficiencies

The compound-specific removal efficiencies for each experiment are shown figure B.3. These figures provide additional detail to the overall ΣPFAS removal efficiencies presented in the main text and were used to evaluate differences between short-chain and long-chain PFAS.

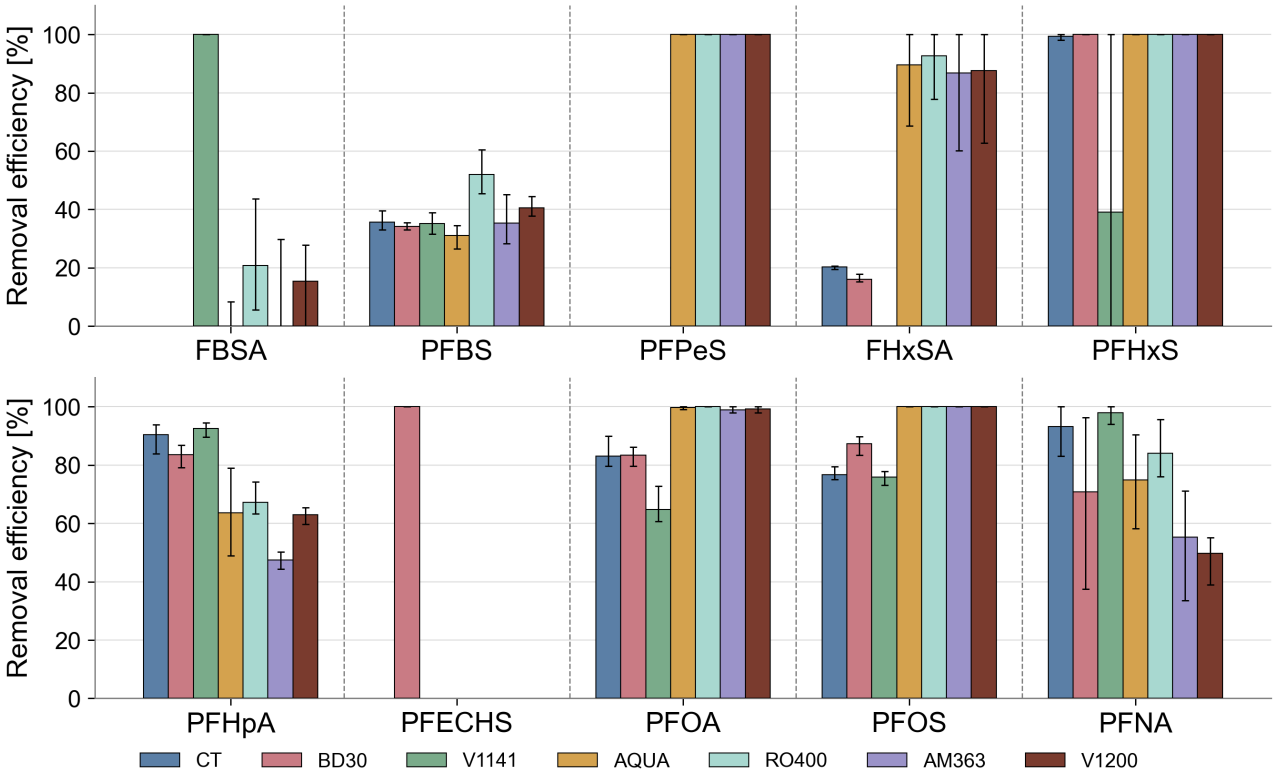

Figure B.3: Compound-specific PFAS removal efficiencies for all experiments. The bars represent the mean removal efficiency, and the error bars indicate the minimum and maximum calculated removal efficiencies.

B.2.3. Compound-Specific Enrichment Factors

The compound-specific enrichment factors are presented in figure B.4. These results show the extent to which individual PFAS compounds were enriched in the foamate compared with the influent. Since enrichment factors were sensitive to foamate concentrations and mass balance closure, these results should be interpreted together with the corresponding mass balance data.

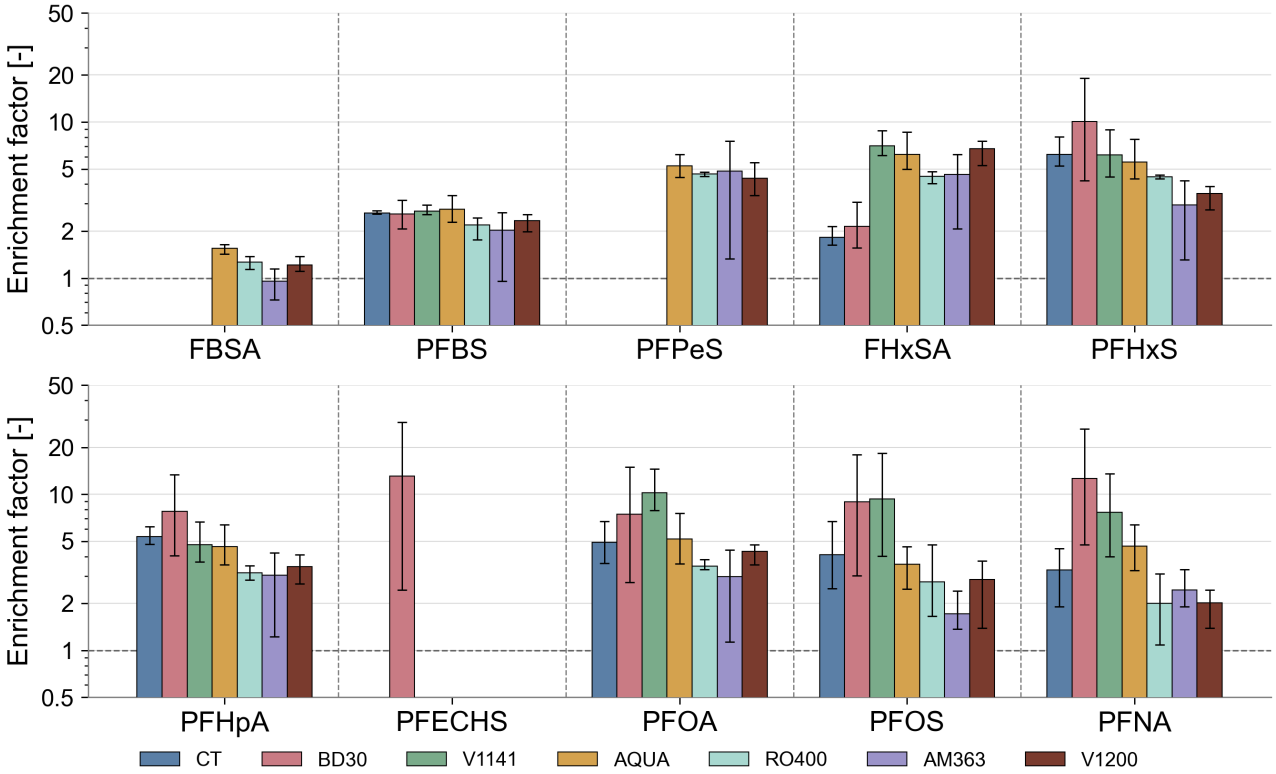

Figure B.4: Compound-specific PFAS enrichment factors for all experiments. The bars represent the mean enrichment factor, and the error bars indicate the minimum and maximum calculated enrichment factors.

B.2.4. Compound-Specific Mass Balance Recoveries

The compound-specific mass balance recoveries are presented in figure B.5. These data were used to assess whether the measured PFAS mass in the effluent and foamate corresponded to the measured influent mass. Deviations from 100% indicate under- or over-recovery and may be related to foamate sampling variability, analytical uncertainty or concentrations close to the LOQ.

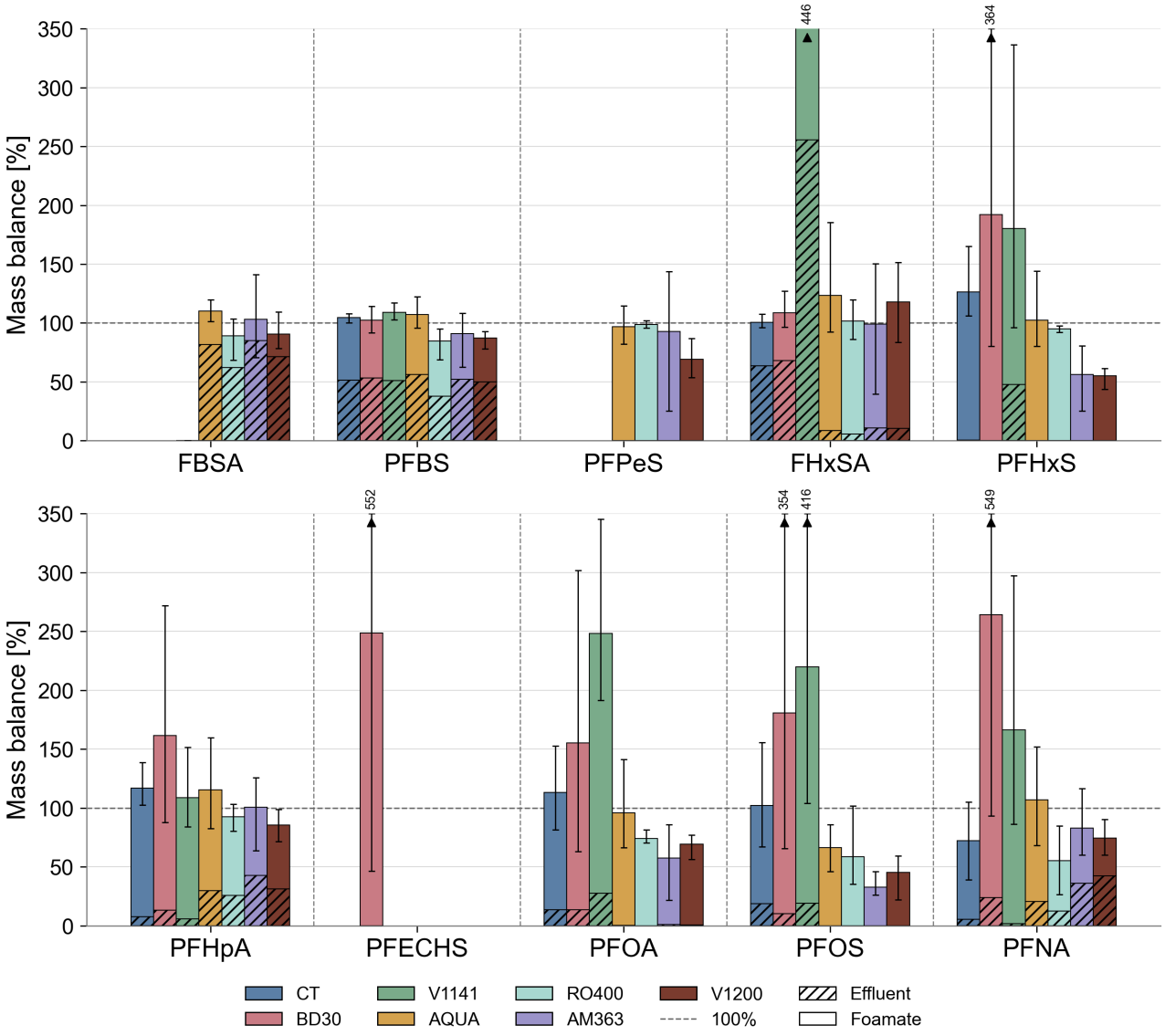

Figure B.5: Compound-specific PFAS mass balance recoveries for all experiments. The bars represent the mean mass balance recovery, and the error bars indicate the minimum and maximum calculated mass balance recoveries.

B.3. PFBS and Foam Conductivity

Figure B.6 presents the relationship between foam conductivity and the mean PFBS concentration measured in the foamate. This comparison was included to support the interpretation of possible matrix effects on short-chain PFAS behaviour during foam fractionation. Since conductivity was not varied as an independent experimental parameter, the relationship should be interpreted as exploratory.

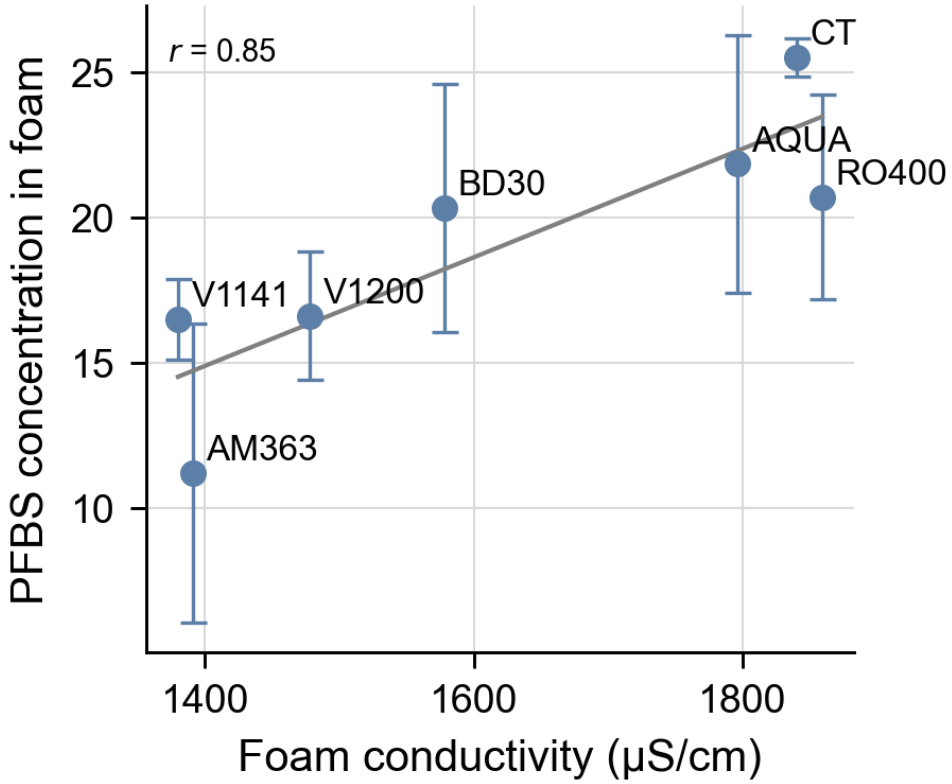

Figure B.6: Relationship between foam conductivity and mean PFBS concentration in the foamate. Each point represents one experimental condition. The relationship should be interpreted as exploratory, since conductivity was not varied as an independent experimental parameter.